AD-A125 870 MOLECULAR BEAM CHEMISTRY: REACTIONS OF OXYGEN ATOMS WITH HALOGEN MOLECULES(U) HARVARD COLL CAMBRIDGE MASS D D PARRISH ET AL. 15 OCT 82 AFGL-TR-82-0313 1/1

UNCLASSIFIED F19628-78-C-0100 F/G 7/4 NL

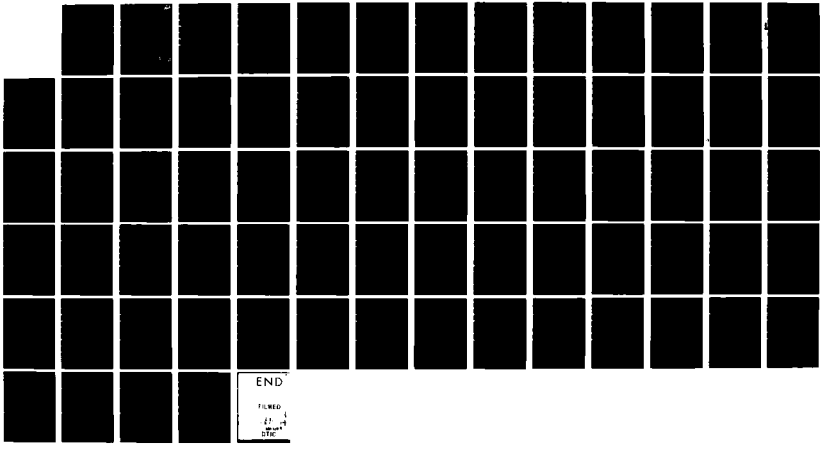

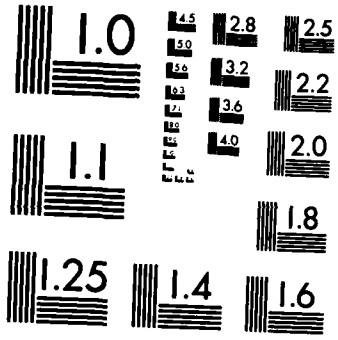

AFGL-TR-82-0313

MOLECULAR BEAM CHEMISTRY: REACTIONS OF OXYGEN ATOMS WITH HALOGEN MOLECULES

D. D Parrish
D. A. Dixon
D. R. Herschbach

Harvard College
Holyoke Center, Box 458
1350 Massachusetts Avenue
Cambridge, Massachusetts 02138

Final Report
1 April 1978 - 30 March 1981

15 October 1982

Approved for public release; distribution unlimited

AIR FORCE GEOPHYSICS LABORATORY
AIR FORCE SYSTEMS COMMAND
UNITED STATES AIR FORCE
HANSCOM AFB, MASSACHUSETTS 01731

Unclassified

SECURITY CLASSIFICATION OF THIS PAGE (When Data Entered)

REPORT DOCUMENTATION PAGE		READ INSTRUCTIONS BEFORE COMPLETING FORM
1. REPORT NUMBER AFGL-TR-82-0313	2. GOVT ACCESSION NO. AD-A125870	3. RECIPIENT'S CATALOG NUMBER
4. TITLE (and Subtitle) MOLECULAR BEAM CHEMISTRY: REACTIONS OF OXYGEN ATOMS WITH HALOGEN MOLECULES		5. TYPE OF REPORT & PERIOD COVERED Final Report 1 April 1978 - 30 March 81 6. PERFORMING ORG. REPORT NUMBER
7. AUTHOR(s) D. D. Parrish D. A. Dixon D. R. Herschbach		8. CONTRACT OR GRANT NUMBER(s) F19628-78-C-0100
9. PERFORMING ORGANIZATION NAME AND ADDRESS Harvard College Holyoke Center, Box 458 1350 Massachusetts Avenue Cambridge, Massachusetts 02138		10. PROGRAM ELEMENT, PROJECT, TASK AREA & WORK UNIT NUMBERS 61102F 2303G2AA
11. CONTROLLING OFFICE NAME AND ADDRESS Air Force Geophysics Laboratory Hanscom AFB, Massachusetts 01731 Monitor/Alfred Rahbee/OPR		12. REPORT DATE 15 October 1981 13. NUMBER OF PAGES 72
14. MONITORING AGENCY NAME & ADDRESS(if different from Controlling Office)		15. SECURITY CLASS. (of this report) Unclassified 15a. DECLASSIFICATION/DOWNGRADING SCHEDULE

16. DISTRIBUTION STATEMENT (of this Report)

Approved for public release; distribution unlimited

17. DISTRIBUTION STATEMENT (of the abstract entered in Block 20, if different from Report)

18. SUPPLEMENTARY NOTES

19. KEY WORDS (Continue on reverse side if necessary and identify by block number)

molecular beams; oxygen atom reactions; electronic structure of reaction intermediates

20. ABSTRACT (Continue on reverse side if necessary and identify by block number)

Molecular beam experiments show that reactions of oxygen atoms with Br_2, I_2, ICl, and IBr proceed via long-lived collision complexes. In the mixed halogen case, a large yield of IO was found, but no ClO or BrO. These results suggest the intermediate complexes are unsymmetrical species, O-Br-Br, O-I-Cl, which are probably stable by greater than 20 kcal/mol and in triplet spin states.

DD FORM 1 JAN 73 1473 EDITION OF 1 NOV 65 IS OBSOLETE

Unclassified

SECURITY CLASSIFICATION OF THIS PAGE (When Data Entered)

MOLECULAR BEAM CHEMISTRY: REACTIONS OF OXYGEN ATOMS WITH HALOGEN MOLECULES

D. D. Parrish,† D. A. Dixon,* and D. R. Herschbach*
Department of Chemistry, Harvard University
Cambridge, Massachusetts 02138

Molecular beam experiments show that the reaction $O + Br_2 \rightarrow BrO + Br$ proceeds via formation and decomposition of a collision complex which persists for many vibrational periods and at least a few rotational periods, or $\gtrsim 5 \times 10^{-12}$ sec. The angle and translational energy distributions agree closely with those predicted by approximate statistical complex models akin to the RRKM theory of unimolecular decay. The analogous reactions of I_2, ICl and IBr were also found to proceed via long-lived complexes. For ICl and IBr a large yield of IO was found, but no ClO or BrO, despite a more favorable reaction exoergicity for these latter products. These results suggest the intermediate complexes are unsymmetrical species, O-Br-Br or O-I-Cl, which are probably stable by >20 kcal/mole and in triplet spin states. The reaction $O + Cl_2$ is found to proceed most likely via an osculating complex. The reactive surface does not sample the well corresponding to C_{2v} OX_2 in its ground singlet state. The complex is predicted to be a linear or slightly bent asymmetric triplet OXX with an electron configuration of either $\cdots(\sigma^*)^1(\pi^*)^3$ or $\cdots(\pi^*)^3(\sigma^*)^1$.

---

†Present address: Metropolitan State College, Denver, Colorado

*Present address: Chemistry Department, University of Minnesota, Minneapolis, MN.

INTRODUCTION

The electronic structure of reactant and product molecules and transition states governs reaction kinetics. While much has been inferred from macroscopic experiments, only single collision studies can hope to examine the actual molecular dynamics.[1] Even such studies may not be able to abstract detailed information about the potential surface.[2] However, significant qualitative electronic structure information about transition states or reaction intermediates can often be obtained. In favorable cases, it is possible to synthesize intermediates.[3] For reactions that proceed through a long-lived complex, even qualitative dynamics can yield information about the stability of these systems that is not presently available from bulk experiments or from electronic structure calculations.

This paper reports a study[4] of several reactions of oxygen atoms with halogen molecules,

$$O(^3P_g) + XY(^1\Sigma^+) \rightarrow OX(^2\pi) + X(^2P_u), \qquad \text{(R1)}$$

with XY = $C\ell_2$, Br_2, I_2, ICℓ, and IBr. Some of these reactions have been examined by classical kinetic methods using flow tubes[5] and diffusion flames,[6] and concurrent molecular beam experiments have been pursued in other laboratories.[7,8] We find that at collision energies of 2-3 kcal/mol these reactions proceed via a long-lived collision complex, except for the $C\ell_2$ case which proceeds via a osculating complex. At higher collision energies there is now evidence that the other O + XY complexes likewise become osculating.[7] Since the ratio of the reduced mass of the reactants to that of the products is rather small, the O + XY reactive scattering proves to be particularly suitable for comparison with simple statistical models. These treat the complex mechanism by phase space[9] and transition state[10] models patterned after the RRKM theory of unimolecular decomposition.[11]

The analogous reactions of hydrogen atoms, methyl radicals, alkali atoms, alkali dimers, alkaline earth atoms, halogen atoms, and mercury atoms with halogen molecules have also been studied in molecular beams.[12] This family of reactions scans the full panoply of reaction dynamics, from extremely impulsive processes akin to photodissociation in the H + XY case[13] to statistical behavior akin to unimolecular decomposition via a well defined intermediates in the Hg + XY case.[14] The O atom reactions have a special place in this family because only they offer the possibility of transitions between triplet and singlet potential energy surfaces. In (R1), the reactants approach on a triplet surface, whereas the products can depart on either a singlet or triplet surface. In accord with qualitative electronic structure arguments,[4] the reactive scattering indicates that these reactions go predominantly via a triplet O-X-Y surface without transition to the singlet X-O-Y surface corresponding to the ground electronics state of the known halogen oxide molecules. This result, interpreted in terms of orbital correlations and electronegativity differences, led to the prediction[4] that the O + F_2 reaction would require a relatively large activation energy even though more exoergic than the other O + XY reactions. This was subsequently confirmed in a flow tube study[6], which found E_{act} = 12 kcal/mol for the O + F_2 case, in contrast to E_{act} = 2 and zero kcal/mol for the Cl_2 and Br_2 systems.

EXPERIMENTAL

The apparatus is schematically depicted in Fig. 1. Only key features and recent modifications will be described here; more details are given elsewhere[9,17]. The two reactant beams cross at an angle of 90° in a large scattering chamber. A 4200 l/sec oil diffusion pump and a large liquid nitrogen cooled shield pump noncondensible and condensible gases, respectively, in this chamber. Reaction products formed in the collision zone are detected by a mass spectrometer mounted on the lid of the scattering chamber. This lid is rotatable allowing the detector to

be moved in the plane of the beams to scan the angular distribution of the scattered reaction products. The detector is comprised of an electron-bombardment ionizer, quadrupole massfilter, scintillation ion counter, and two gated scalars synchronized with the modulation of the halogen molecule beam. In the velocity analysis experiments, a slotted disk chopper is attached to the lid between the collision zone and the detector. A PDP 8/L computer is used both as a multiscalar to record the time of flight (TOF) spectrum of the products and for immediate, approximate extraction of the velocity distribution from the recorded spectrum.

To reduce the residual partial pressure of background product molecules in the ionization region of the detector to a low level ($\lesssim 10^{-14}$ torr) the ionizer is nested in three chambers differentially pumped by 50 l/sec ion pumps. The ionizer is surrounded by liquid nitrogen cooled surfaces and the design allows unionized product molecules ($\sim$99.9% of the total) to "fly through" the ionizer. A new pump element which is a 46 cm x 2.5 cm x 0.32 cm gold plated copper strip cooled to $\sim 15^{\circ}$K by an Air Products and Chemicals Inc., Displex Model CS-202 closed cycle, displacer/expanded helium refrigerator has been added. The 15°K element is completely surrounded by $\sim 77^{\circ}$K radiation shields cooled by the refrigerator's first stage. The refrigerator is mounted at the throat of the ionizer chamber ion pump and the pumping element extends down this chamber to within 13 cm of the ionizer. This refrigerator has given more than 6000 hours of maintenance free operation.

Beam Sources. The oxygen atom beam is produced by a low pressure ($\lesssim$100 microns Matheson Extra Dry oxygen) microwave discharge. The source shown in Fig. 2a is similar to that used previously for deuterium atoms[9] and chlorine atoms[18]. The discharge cavity is essentially the foreshortened 1/4 wave coaxial cavity described by Broida and coworkers[19]. However, for convenience of mounting and vacuum connections, a wave guide has been added by lengthening the inner and

outer electrodes of the cavity by four wavelengths. The discharge occurs in a quartz tube which is sealed into the gold plated copper waveguide with epoxy resin to provide a vacuum tight seal. Water cooling coils protect the epoxy from pyrolysis while air cooling prevents melting the quartz tube. Two important requirements for satisfactory operation have been identified: the quartz tube must be coated with freshly prepared, syrupy phosphoric acid before each run, and the dimension indicated by A in Fig. 2a must be held as small as possible. The microwave frequency is 2450 MHz and is operated at ~100 watts power. The beam exit slit (1 mm x 10 mm) is located ~2 cm from the center of the cavity. Since the beam is taken from the region of active discharge it could be expected to contain significant amounts of O_2 ($^1\Delta$) and $O(^1D)$ metastable species in addition to ground state $O(^3P)$ atoms. The $O_2(^1\Delta)$ is unreactive at the experimental collision energy with the halogens as all reactions are at least 16 kcal/mole endoergic. The $O(^1D)$ is, however, generally quite reactive and would, if present, possibly interfere with the observation of the products of ground state O atom reactions. However, the ^1D state is efficiently collisionally quenched[20] by O_2 and is thus not expected to be a significant component of the beam; indeed, we have seen no evidence for reactions of this excited species as is discussed later. Velocity analysis of the beam indicate that it is translationally hot (1000° to 1200°K) with a full Maxwellian velocity distribution. The fluxes of O and O_2 are approximately equal under our optimum discharge conditions.

The halogen molecule source shown in Fig. 2b is a high pressure (150 to 900 torr) supersonic nozzle[21]. The nozzle is fabricated from a 6.2 mm O.D quartz tube pulled down to form a short closed tip. This tip is ground back until a 0.10 to 0.17 mm dia orifice is produced. A heating mantle around the quartz tube allows the nozzle to be operated from 300° to 1000°K. The nozzle is moveable along the beam axis and is mounted at an optimum value of ~7 mm behind a 1.5 mm skimmer.

The nozzle beam chamber is pumped by a large liquid nitrogen cooled shield and a 2400 l/sec oil diffusion pump to achieve the very high pumping speeds required. The resolution of the velocity analyzer is insufficient to verify the very narrow velocity distributions expected for this beam. The velocity analysis is consistent with high Mach numbers (>10) and nearly complete relaxation of the rotational degrees of freedom of the halogen molecules.

Both beam sources are mounted in chambers differentially pumped by 1200 l/sec oil diffusion pumps. Collimating slits (1.25 mm x 10 mm) lead to the scattering chamber. The measured angular widths of the resulting beams are 5° (full width at half-peak intensity). Detailed calculations indicate this is the maximum size consistent with a scattering region cross-section small enough to be completely viewed by the detector. A rotating paddle modulates the halogen beam at 70 Hz and a beam flag is used to interrupt the oxygen atom beam. The beam modulator and the beam flag are located in the respective differentially pumped chambers.

Experimental Procedures. The angular distributions are obtained (with the TOF chopper removed) by counting at each laboratory scattering angle for a period of 20 to 200 sec with the beam flag open and then immediately for the same period with the beam flag on the O atom source closed. The modulated signal (difference between "on" and "off" scalars) with the beam flag closed is subtracted from the open beam flag modulated signal to obtain the reactive scattering intensity. In the studies reported here the closed beam flag signals were typically 0 to 30% of the beam flag open signals and were angular dependent, increasing to a maximum near the chopped halogen beam; these beam flag closed signals can be attributed to the reaction of the halogen molecules with background oxygen atoms in the scattering chamber. The backgrounds ("off" scalar) were 1 to 20 times larger than the reactive signals. To obtain the angular distributions four separate scans through the complete angular range were made in varying angle sequence. Since each data

point was relatively noisy, the time variation in the signal at each angle was included in the procedure developed to time normalize for beam intensity or detector sensitivity variations during the experiment. This method is described in the Appendix. It gives significantly better data than the traditional method of using the time variation of the signal at a single, relatively noise-free angle for normalization. The time normalized signals were averaged over the four angle scans to obtain the data points. Simple error propagation techniques are described in the Appendix which allowed the systematic derivation of confidence limits and error bars.

The TOF velocity analysis data are collected in the manner described previously.[9] A slightly narrower chopper disk slit width (0.15 cm) yielded a shutter function of 0.067 τ_c (full width at half maximum) with a chopper period τ_c of 860 μsec and channel width of 24 μsec. Some improvements have been made in the procedure[9] for converting the TOF spectrum to the velocity distribution. At low velocities (long flight times), the velocity resolution ($\Delta v/v$ with Δv the FWHM at nominal velocity v) is determined primarily by the ratio of ionizer length (2.5 cm) to length of flight path (13.5 cm) and is relatively unaffected by the TOF channel width. Hence, two or more consecutive channels at the end of the TOF spectrum can be combined by adding the counts in each; the analysis with the resulting longer channel width gives improved signal-to-noise ratios with only a small decay in velocity resolution. In practice, the data were analyzed by beginning with the last channel and combining with preceding channels sequentially until the product of the velocity resolution and the noise-to-signal ratio was minimized. This process was then repeated with each channel. Error propagation techniques again allowed assignment of systematic error bars. The low velocity data exhibit less scatter than would be expected from the magnitude of the error bars. This phenomenon arises because consecutive points come from overlapping

time periods and hence include much of the same data. The error bars do, however, indicate the random errors in the data.

RESULTS

Table I gives the important parameters that varied between experimental runs. For a given reactant system, identical conditions were maintained as closely as possible for the angular velocity distribution runs. The measured product angular distributions are shown in Figs. 3 and 4 along with curves calculated from the statistical complex models discussed later. In all cases the angular distribution peaks near the direction of the nominal centroid vector.

The $O + Cl_2$ distribution, however, does exhibit a slight shift toward the O atom beam. These experimental angular distributions exhibit no clear indication of the bimodal structure generally associated with a collision complex mechanism. This lack of structure is due to the inability of the experiments to resolve the two peaks which, for these systems, are very close together in angular range. As discussed below this behavior is clearly understood and, indeed, is directly predicted by the collision complex model.

Careful searches were made for the other possible product (ClO from O + ICl and BrO from O + IBr) from the mixed halogen reactions, but no indications of these products were found. Energetic considerations (Table II) do not prohibit the formation of these alternative products and statistical phase space theory predicts that ClO should be the dominant product of the O + ICl reaction. Figure 5 indicates the sensitivity of the detector for the ClO product and shows that the signal from this product must be at least one order of magnitude less intense than expected from the statistical complex model assuming a distribution of products from phase space theory. The low intensity of the signal from the O + IBr reaction prevented a definitive search for the BrO product from this reaction.

The measured product velocity spectra are shown in Figs. 6-8 along with curves calculated from the statistical complex models for the reactions $O + Cl_2$, $O + Br_2$ and O + ICl. Signals were so small for the $O + Cl_2$ reaction (the single velocity distribution required 3 hr.) that only one velocity distribution near the peak of the angular distribution was measured. For the $O + Br_2$ and O + ICl reactions each of the independently measured velocity distributions are normalized to a common intensity scale by requiring that the integral of the velocity distribution, when converted to number densities, equals the scattering intensity at the corresponding angle in the angular distribution measurements.

A small amount of background halogen molecules effuses from the differentially pumped halogen source and is, thus, modulated. This background is very much smaller than the beam intensity but the reaction of O atoms with this background can dominate the detected product signal at some ranges of laboratory angles and velocities. This effect is evident at low laboratory velocities and angles wide with respect to the centroid ($\theta = 102^{\circ}$ and 25°) for the $O + Br_2$ reaction. This accounts for the wide deviations from the model calculations at these angles; the low velocity peak at $\theta = 25^{\circ}$ could be attributed to this reaction with background molecules. Another possible explanation is due to the presence of van der Waals dimers in the halogen nozzle beam. Some dimers are expected due to the high source pressures.

The reaction

$$O + (X_2)_2 \rightarrow OXX + X_2$$

could occur and the OX_2 could fragment in the ionizer due to electron bombardment or could decay to OX+X before being detected. This could also account for the low velocity peak at $\theta = 25^{\circ}$.

In all cases the velocity distributions peak at velocities that correspond closely to forward (0^o) or backward (180^o) scattering in the center of mass system and fall off gradually toward the energy conservation limits. Poor velocity resolution of the products as well as energy and angular spreads in the parent beams account for the intensity in energetically excluded regions. If the parent O atom beam had a significant proportion of metastable $O(^1D)$ atoms which produced interfering products, the excess energy would allow scattering at higher laboratory velocities. The lack of such scattering and the reasonably good agreement of the loose transition - state model which assumes only ground state O atoms with the data at high velocities preclude a significant contribution of products from $O(^1D)$ reactions.

Kinematic Analysis. The transformation of the flux density I_{LAB} in the laboratory (LAB) system to the flux density I_{CM} in the center-of-mass (CM) system is given by

$$I_{CM}(\Theta,u) = (u^2/v^2)\ I_{LAB}(\theta,v)$$

where u and Θ are the velocity and angle in the CM system and v and θ the respective values in the LAB system. This direct transformation with no averaging holds true only for monoenergetic beams. For the $O + Br_2$ reaction the kinematics are favorable enough and the data are complete enough to allow this transformation to be made with reasonable accuracy if the spread in the reactant beam velocities is ignored. This is accomplished by assigning each beam its most probable velocity. Figure 9 shows the results of this nominal transformation of the data for $O + Br_2$ from Fig. 7 with some smoothing of the contours. Elementary considerations of the

collision process dictate that the scattering must be cylindrically symmetric about the relative velocity (the 0^o - 180^o axis) and the data showed this within experimental uncertainty. The data before smoothing showed a slightly greater intensity in the CM angular range 90^o to 180^o which was within experimental uncertainty. A reaction which proceeds through a complex[22] whose lifetime is less than several rotational periods would be expected to yield an angular distribution with some asymmetry about $\theta = 90^o$, but in such a case the 0^o to 90^o quadrant would have higher scattering intensity, just opposite to the apparent asymmetry we observed. For our map, we assumed symmetry about the $\Theta = 0^o$ and 180^o line and about $\Theta = 90^o$. These data, combined with smoothing, energy conservation considerations, and the fact that the contours must be perpendicular where they cross the 0^o - 180^o axis and the 90^o ray give the map shown in Fig. 9. The bimodal structure of the scattering intensity is clearly apparent with the most intense scattering distributed approximately symmetrically forward and backward with respect to the initial O atom direction.

The CM angular distribution for the O + Br_2 reaction may be obtained from Fig. 9 by integrating the scattering at each angle over the product velocity. This result is presented in Fig. 10(a). The CM velocity distribution at any angle may be obtained by taking a cut through the contour plot of Fig. 9 at the chosen angle. At all angles the results are very nearly identical. Figure 10(b) shows the CM velocity distribution that best fits all angles; Fig. 10(c) gives the product translational energy distribution that corresponds to this velocity distribution.

Total Reaction Cross Sections. The total reactive cross section could be easily derived if it were possible to measure the absolute beam densities and the volume of the beam intersection region. However, this determination is not possible here nor has it been in any crossed molecular beam study. Thus indirect methods are usually employed; the most common is comparison of measured small

angle elastic scattering with theoretical predictions to normalize the experimental intensity scale to absolute values.[23] For these studies, however, such a comparison is not possible. Elastic scattering of O atoms cannot be separated from the mass 16 detector background and mass 16 contributions from the elastic scattering of the O_2 component of the O atom beam. The elastic scattering of the halogen molecules may be measured, but the scattering comes from the O_2 as well as O in the O atom beam, and the kinematics for interpreting this scattering is particularly poor.

A crude estimate of the total cross section may be obtained from comparing the relative reactive and elastic signal intensities for these reactions with the halogen atom-halogen molecule exchange reactions.[18] This comparison indicates the cross sections are the same order of magnitude for the two reaction families, roughly about 10 $\mathring{A}^2$.

STATISTICAL COMPLEX MODELS

A center of mass angular distribution which is symmetric about $\theta = 90^o$ is suggestive of a reaction which proceeds through a collision complex, but is not a sufficient condition. If a complex persists for several rotational periods and many vibrational periods, all "memory" of the initial conditions of complex formation are lost. Only total energy and total angular momentum are conserved. This situation permits simple statistical models to be substituted for detailed studies of collision dynamics. Many statistical approaches have been developed including phase space models[24] and transition state models.[13,22] These models are descendants of the transition state (RRKM) treatment of unimolecular decomposition[14] and the compound nucleus treatment of nuclear fission.[25] Approximate transition state models will be briefly discussed and applied to the reaction systems under study here.

Approximate Product Velocity Distribution. The total energy available to the reaction products is

$$E_{tot} = E + W + \Delta D_o = E' + W' \qquad (2)$$

where E and W denote the initial relative translational energy and internal excitation of the reactants, E' and W' are the corresponding quantities for the products and ΔD_o is the reaction exoergicity. The role of the statistical models is to partition this total energy, weighted by the density of energy levels or states, among the degrees of freedom of the dissociating complex. According to the simplest transition state model[13], the translational energy distribution is given by

$$P(E') = A(E')N^+(E_{tot} - E') \qquad (3)$$

The N^+ factor is the energy level density of "active" vibrations and rotations at the critical configuration of the complex. The A factor takes into account the centrifugal effects associated with complex formation and decomposition.

The classical approximation,

$$N^+(E_{tot} - E') = (E_{tot} - E')^n \qquad (4)$$

is appropriate here because the zero point energies are small and similar for reactants, complex, and products. The exponent n is given by $n = s + \frac{1}{2}r - 2$, where s and r, respectively, denote the number of vibrational modes and active rotations at the transition state. The number of modes assigned to s and r depends on the geometry and bonding assumed for the transition state. For a "tight" (all atoms bond in a single "molecule") three atom complex, a linear structure has s = 4, r = 0, and n = 2; a nonlinear one has s = 3, r = 1, and n = 3/2. In the "loose" complex the bending modes go over to free rotation of the product diatomic molecule; thus s = 1, r = 2, and n = 1.

In general the calculation of the A factor is quite complex because the details of the angular momentum coupling must be analysed. The magnitude and

direction of the total angular momentum is conserved in the collision;

$$L + J = J = L' + J' \tag{5}$$

where L and L' are the angular momenta associated with centrifugal motion of the reactants and products ($L = \mu v b$ where μ is the reduced mass, v is the velocity and b is the impact parameter) and J and J' the rotational momenta of the reactant and product molecules, respectively. To avoid consideration of the convolution of the unknown component momenta distributions, the simplest approach[13] is to assume that the centrifugal angular momentum dominates:

$$L \sim J \sim L' \tag{6}$$

As discussed later, this is at least valid for the entrance channel. If the transition states for formation and decomposition of the complex are taken as the centrifugal barriers in the entrance and exit channels, respectively, and if these barriers lie sufficiently far out to be governed by the r^{-6} van der Waals attraction, then

$$\begin{aligned} A(E') &= (E'/B_m')^{2/3}, \quad E'<B_m' \\ &= 1 \qquad\quad , \quad E'>B_m' \end{aligned} \tag{7}$$

The parameter B_m' is the maximum exit centrifugal barrier and can be calculated if C and C', the van der Waals force constants in the entrance and exit channels are known,

$$B_m' = (\mu/\mu')^{3/2} (C/C')^{\frac{1}{2}} E_t. \tag{8}$$

Here μ and μ' are the reduced masses of the reactants and products. In Eq. (4) n has been set equal to 2 corresponding to tight linear complexes. The dotted curve in Figure 12(c) compares this result for the $O + Br_2$ reaction with the experimentally derived distribution; Figure 12(b) compares the corresponding product velocity distributions.

Product Angular Distribution. In the angular momentum limit given by

Eq. (6), the CM angular distribution is given by the simple expression

$$I(\Theta) = \frac{1}{2\pi^2 \sin\Theta} \qquad (9)$$

The curve given by Eq. (9) is compared with experiment in Fig. 10a; it is clearly much too strongly peaked even with allowance for the imperfect experimental angular resolution. The less sharply peaked experimental curve must result from the failure of Eq. (6) at least in the exit channel. In the entrance channel (complex formation) the centrifugal angular momentum must indeed dominate because the rotational excitation of the reactant halogen molecule is very small due to the rotational "cooling" which takes place in the expansion of the nozzle beam. Detailed consideration of the energetics and angular momentum conservation in the product channel, however, indicate that the rotational angular momentum of the diatomic product cannot be neglected. Equation (6) must be replaced with

$$\underset{\sim}{L} + \underset{\sim}{J} = \underset{\sim}{L}' + \underset{\sim}{J}' \qquad (10)$$

As a result the final relative velocity of the products is not constrained to be perpendicular to J. The peaking predicted by Eq. (9) must then be rounded off.

A transition state treatment has been developed[22,26] to provide a simple algorithm for calculating the shape of the angular distribution. Three parameters are required: L_m, the maximum orbital angular momentum with which the complex can be formed (at the given collision energy); M_o, the root-mean-square projection of the total angular momentum on the initial relative velocity vector; and M_o', the corresponding projection on the final relative velocity vector. If the ratios L_m/M_o' and M_o/M_o' are specified, the angular distribution can be read from reduced plots prepared by Miller.[27] Application of this model for the angular distribution to these chemical systems is inconsistent, however, since equation (10)

dictates that $M_o = 0$ and $M_o' \neq 0$. The tight linear complex assumed in calculating the product velocity distribution also implies that M_o' must equal zero. Thus, applying this traditional transition state model would be essentially an empirical fit of the model to the experimental data. This is the approach that was followed in the initial communication of this work. The $O + Br_2$ angular distribution was nicely fit by the model when the ratio L_m/M_o' was set at approximately 2.[4] Another inconsistency is that in order to calculate L_m and the A factor in the product translational energy distribution it was assumed that the formation and decomposition of the complex is governed by the centrifugal barrier associated with the r^{-6} van der Waals attraction. This means that at the transition state the complex must correspond to an atom and a diatomic molecule interacting only through weak, non-directional forces. Clearly this corresponds to a "loose" complex rather than the "tight" linear complex assumed in deriving the product velocity distribution.

Loose Transition State Model. To avoid the problems discussed in the preceding section, the simple models assuming a tight complex have been abandoned. A model for a three atom "loose" complex constrained only by Eq. (10) can be used to obtain both the product velocity and angular distributions. This model still assumes that the critical configurations are the centrifugal barriers but considers in detail the conservation of both energy and angular momentum. The final result is a classical analog of the quantum phase space theory;[24] every state of the complex at the critical configuration that conserves energy and angular momentum is weighted equally. If the van der Waal's force constants can be obtained and if the structural parameters of the reactant and product diatomics are known, the model contains no adjustable parameters. All observable properties of the reaction may be predicted including product velocity and angular distributions, total reaction cross sections, and branching ratios of complex decomposition to reactant channel and product channel(s).[28] This model will be described fully elsewhere.[16]

Table II contains the parameters used in the model calculations. The van der Waals force constants for the r^{-6} interaction, C, are obtained from the Slater-Kirkwood approximation.[29] The effective number of electrons were taken to be 6 for the O atom, 14 for halogen molecules, 7 for halogen atoms, and 13 for halogen monoxide diatomic molecules. The polarizability values were chosen to be consistent with literature values and atomic additivity.[30] The polarizabilities (in $\mathring{A}^3$) were taken as 0.77 for the oxygen atom[31] and 2.3, 3.1, and 5.2 respectively for the Cl, Br, and I atoms.[30] The value for each diatomic molecule was obtained by summing the polarizability of each substituent atom. The induction terms were calculated using dipole moments (in D) of 1.24 for ICl[32], 0.9 for IBr[33], and 1.26, 1.61, and 2.45 respectively for ClO, BrO, and IO.[34] The reactant internal excitation W was calculated from the beam temperatures in Table I assuming classical rotation and that in the nozzle expansion no vibrational relaxation occurs, but that 80% of the rotational energy is converted to translational energy. (This assumption is consistent with the measured velocity distributions of the reactant beam.) The bond energy D_o for each molecule was taken from standard references[35,36] with the exception of IO which will be discussed in a later section. The diatomic spectroscopic vibrational constants ω_e and rotational constants B_e were taken from Ref. 36.

As shown in Fig. 10a, the angular distribution calculated at a nominal collision energy of 2.11 kcal/mole gives excellent agreement with the CM angular distribution obtained by the nominal transformation of the experimental data. The anisotropy ratio β (equal to the ratio of intensity at $\theta = 0^\circ$ or 180° to that at $\theta = 90^\circ$) predicted by the model is 2.6 as compared to 2.3 obtained from the nominal LAB → CM transformation. The angular distribution obtained in another study[7] at a lower reactant translational energy (0.8 kcal/mole) indicated a smaller value for β. This is in qualitative accord with the model which predicts $\beta = 1.9$ at 0.75 kcal/mole.

In contrast to the good agreement found for the angular distribution, however, Figs. 10(b) and 10(c) indicate that the predicted product velocity distribution is in poor agreement with experiment. The loose transition-state model predicts too large a fraction of the total available energy entering product translational energy.

Comparison With Laboratory Data. Comparison of the model predictions with the curves derived from the nominal CM to LAB transformation may, however, be misleading. The models are formulated in the center of mass system for a complex of given total energy formed in a collision with specific relative translational energy. The experiments, however, were run in crossed molecular beams and the O atom beam was not velocity selected so a wide range of initial translational energies was present in the experiment. Of less importance is the range of the total energy of the complex with respect to separated products caused by this spread in translational energies as well as a small range of internal excitation in the reactant diatomic molecule. Since no method presently exists to deconvolute the angular and energy distributions from the energy spreads and to unambiguously transform the data to the CM system, a different approach will be taken. The model predictions will be averaged over the initial conditions and then transformed to the LAB reference frame to be compared directly with experiment. Formally, this transformation may be expressed as

$$I_{LAB}(\theta,\underline{v}) = \int_0^\infty dv_1 \int_0^\infty dv_2\, n_1(v_1)\, n_2(v_2)\, (\underline{v}^2/\underline{u}^2)\cdot V\cdot \underline{V}(V)\, I_{CM}(\Theta,\underline{u};V) \quad (11)$$

Here $I_{LAB}(\Theta,\underline{v})$ is the flux of the observed product of laboratory angle and velocity $\underline{v}$. $I_{cm}(\Theta,\underline{u};V)$ is the center of mass product flux predicted at CM angle Θ and velocity $\underline{u}$. This CM flux is a function of the relative velocity of reactant approach $V = (v_1^2 + v_2^2)^{1/2}$ when angular divergence of the beams is neglected. The velocity number distributions in the beam are given by $n_1(v_1)$

and $n_2(v_2)$. The Jacobian for the CM to LAB transformation is simply $\underline{v}^2/\underline{u}^2$. Finally, $\underline{V}(V)$ gives the dependence of the total cross-section for complex formation Q_c on the relative velocity.

The function $I(\Theta,\underline{u};V)$ may be calculated from the loose transition-state model. Here for convenience an approximation is made. The assumption

$$I(\Theta,\underline{u};V) \sim I(\Theta;V)\ \underline{U}\ (\underline{u};V) \tag{12}$$

is made that the CM velocity distribution is independent of scattering angle as given by (12). Except at the limit of $\underset{\sim}{L} = \underset{\sim}{J} = \underset{\sim}{L}'$ this cannot be rigorously true, but it is expected to be a good approximation for these studies. This expectation is strengthened by inspection of Fig. 10(a) where this separability appears to hold within the uncertainty of the data. It has also been assumed that $I(\Theta,\underline{u};V)$ is independent of internal state of the reactant diatomic molecule over the small range present in the experiment. Average values for the internal vibrational and rotational energies can then be assigned.

The dependence of Q_c on relative velocity is a direct consequence of the loose transition-state model. The total cross section is determined by the largest impact parameter that still allows the colliding species to surmount the centrifugal barrier; thus

$$Q_c = 3/2\ \pi\ (2C/E)^{1/3} \tag{13}$$

for the assumed van der Waals interaction which gives

$$\underline{V}(V) \propto V^{-2/3} \tag{14}$$

to substitute into Eq. (11).

The halogen beam produced from the nozzle expansion has a very narrow velocity distribution; therefore averaging over the velocity distribution of this beam is not necessary.[37] Finally, no attempt is made to calculate the absolute magnitude of the laboratory scattering. The final calculation will be normalized to the

laboratory data. With these approximations Eq. (11) simplifies to

$$I_{LAB}(\Theta,\underline{v}) \propto \int_0^\infty dv_1\ n_1(v_1)\ (\underline{v}^2/\underline{u}^2)\ V^{1/3}\ I(\Theta;V)\ U(\underline{u};V) \qquad (15)$$

The calculation is accomplished by selecting nine velocities, equally spaced over the velocity range of the oxygen atom beam.[38] At each of these velocities $I(\Theta;V)$ and $(\underline{u};V)$ are calculated. $I_{LAB}(\Theta,\underline{v})$ is then calculated for all desired product laboratory angles and velocities and then summed over the nine reactant beam velocities. The results for the loose transition-state model are given for the angular distributing by the solid curves in Figs. 3 and 4, and for the velocity distributions by the solid curves in Figs. 6-8. It should be emphasized again that, except for the single normalization constant, no adjustable parameters are included in the calculations.

Figure 11(a) compares the angular distributions predicted by the model for the five reaction systems. These distributions are for the oxygen atom velocity which gave the greatest contribution to the total reactive scattering in the integration over the oxygen atom velocity. The corresponding collision energies were 3.92, 2.11, 2.44, 2.43, and 2.41 kcal/mole for the O + Cl_2, Br_2, and I_2, ICl and IBr reactions, respectively. The anisotropy ratios calculated for the O + I_2 and ICl reactions are 1.9 and 2.8 respectively, which are in good agreement with the respective empirical values of 1.7 and 2.5 obtained in Ref. 7. The values of Grice et al[7] are lower for two reasons: those experiments were run at lower collision energies where the anisotropy ratio is expected to be lower and the convenient mathematical function used in Ref. 7 was a two term Legendre polynomial expansion which rounds the CM angular distribution at $\Theta = 0^\circ$ and 180° and thus underestimates the anisotropy ratio.

The CM to LAB calculations were repeated using the same angular distributions from the loose transition-state model but using the velocity distributions corresponding to the energy distributions from Eq. (3) for a tight complex (n = 2).

Figure 11(b) compares these energy distributions for the five reaction systems. The results of these calculations are shown by the dashed curves in Figs. 3, 4 and 6-8.

DISCUSSION: DYNAMICS

$O + Br_2$ and $O + I_2$ Reactions. The laboratory angular distributions calculated from the statistical complex models are in at least qualitative agreement with the data for these two reactions. The angular distributions appear in the correct angular range and have shapes similar to the experimental distributions. The calculations for the loose collision complex are not peaked sharply enough, but the calculations for the self contradictory model composed of the angular distribution for a loose complex and the velocity distribution for a tight complex give nearly quantitative agreement. The velocity distributions for the $O + Br_2$ reaction show the same results: the "hybrid" model gives results that agree in shape and in position with experiment while the loose collision complex predicts too much high velocity product.[39] The agreement of the model calculations with the LAB data, with the nominal CM distributions for $O + Br_2$, and with the anisotropy ratios extracted in an independent investigation[7] clearly show that the angular distributions are predicted very nearly exactly by the loose collision complex model while the velocity distributions are accurately given by the approximate tight, linear complex model. Grice and coworkers[7] also found that a tight, linear complex best fit their $O + I_2$ velocity analysis data and was in accord with their $O + Br_2$ data. The angular distributions obtained by Grice et al[7] for the $O + Br_2$ and $O + I_2$ reactions are very similar to those obtained in this study, even though their initial translational energy was somewhat lower [40] although our angular distribution for the $O + I_2$ reaction is better resolved than that of Grice et al.[7] Comparison of velocity spectra is not possible as we did not obtain this data for the $O + I_2$ reaction and Grice et al[7] did not obtain velocity spectra for the $O + Br_2$ reaction.

The apparent contradiction between the angular distribution and velocity distribution models cannot be easily avoided by assuming that the product velocity distribution is "fixed" early in the exit channel when the incipient products are still interacting strongly (tight complex) while the angular distribution is determined at the exit centrifugal barrier where a "loose" complex must be the proper description. In order to calculate the angular distribution from the loose complex all values of L' (product orbital angular momentum) consistent with the conservation laws are weighted equally. Since L' is related to final relative product velocity V' by

$$L' = \mu' V' b'$$

where b' is the final asymptotic impact parameter of the departing products, only the velocity distribution from the loose collision complex model is consistent with that angular distribution unless some ad hoc assumption concerning the distribution of b' is made. Clearly a more unified model is desirable, but for these systems the angular and the velocity distributions can be adequately calculated from the separate and contradictory models.

These experiments are particularly sensitive to products produced with low velocities in the center of mass system. This arises because the Jacobian factor given in Eq. (1) greatly magnifies this scattering when it is observed in the laboratory system. The approximate transition-state model predicts that these reaction systems will give a particularly large amount of low velocity products as may be seen from inspection of Eq. (7) and (8). The ratios μ/μ' and C/C' are both much smaller than unity, so the energy distributions peak at very low values as shown in Figure 11(b). This effect is responsible for the lack of any clearly bimodal LAB angular distributions that usually characterize reactions that proceed through collision complexes. Even though the C/C' ratio enters Eq. (8) only to the ½ power, the Jacobian factor so magnifies the low

velocity scattering that the data is quite sensitive to the value of this ratio. The fact that the ratios calculated for these experimental systems do give adequate fits to the data indicates corroborates our choice of the critical configurations for complex information and decomposition as being the centrifugal barriers where the interaction between reactants or products is adequately given by the van der Waals interaction.

There are two important factors which vary with relative collision energy in the model calculations. These are the cross section for complex formation and the complex decomposition branching ratio between reactant and product channels. At low collision energies the complex formation cross section is larger (see Eq. (13).) The fraction of complexes decomposing into the exoergic product channel rather than reforming reactants is also greater. Low energy collisions give scattering near the halogen beam, near $\theta = 90^{\circ}$ in the LAB. If either of these factors is neglected, the model predicts that the angular distribution would have nearly the same shape but would appear at smaller laboratory angles than the data show. These results also give more confidence in the statistical complex model in general and the centrifugal barrier as the critical configuration in particular.

$O + Cl_2$ Reaction. For this reaction, the agreement between our model and experiment is not nearly as quantitative. The angular distribution appears to be centered at smaller laboratory angles than predicted by the statistical complex models. This feature could be taken to indicate that collisions of high velocity reactants which give scattering at smaller laborabory angles are more likely to yield reaction than low velocity collisions. This would be consistent with the experimental study[5a] which found that this system has an activation energy of 2.9 kcal/mole. To quantitatively verify this, the calculations for the "hybrid" model were repeated with the inclusion of an approximate treatment of an energy barrier in the entrance channel. At a reactant separation of 3.4 $\mathring{A}$ (roughly

the distance expected from the atomic radii), only the collisions with translational energies along their line of centers greater than 2.9 kcal/mole were allowed to form complexes. It was not possible to easily account for complexes decomposing to reactants so the variation of branching ratio with collision energy was neglected. This approximate treatment gave the dash-dot curves in Figs. (3) and (6). The predicted angular distribution is in better agreement with experiment insofar as the general position is concerned, but it is still not peaked sharply enough. The predicted velocity distribution, however, shows too much high velocity product to agree with experiment.

The O + Cl_2 reaction has been studied by Grice et al[7d,e] at two different initial translational energies, nominally 3.0 and 6.9 kcal/mole, using a seeded oxygen nozzle beam. These workers find that the reaction proceeds via an osculating complex[41] with a ratio of backward to forward CM peaks of 0.30 at the higher translational energy and an increased ratio of 0.55 at the lower energy. Our initial translational energy ($\sim$2.9 kcal/mole) is comparable to their lower energy study and coupled with the presence of the modest activation energy the angular distributions should be quite similar. Although they[7a] did not publish a LAB angular distribution, our LAB result would be quite similar to theirs in that we do show a larger forward peak as compared to the backward peak. As we did velocity analysis at only one angle (forward peak) we could not construct a full CM map and thus cannot compare directly with Grice et als CM angular distribution. We do note that they only obtained velocity analysis at two angles at the lower energy which did not give a full CM map either. Grice et al[7e] found that there was a dependence of CM velocity distribution on scattering angle and suggested that two components were present, one proceeding by a stripping-like process and one proceeding via the osculating complex. Our study, in agreement with the work of Grice et al[7d] at the higher

collision energy, predicts too much high velocity products. This is somewhat surprising for a system proceeding by an indirect process with a more direct proce superimposed on it. One would expect to see more high velocity product whereas we find the opposite. Although it is likely that the reaction proceeds via an osculating complex, the quantitative determination of the details of the $O + Cl_2$ reactive scattering in the threshold region awaits further experiments.

O + ICl and I + IBr Reactions. These two reactions are complicated by the presence of two potential product channels: IO + Cl or Br and ClO or BrO + I. Despite careful searches, only the IO product has been observed in each reaction. Figure 5 indicates that at least in the case of O + ICl, the ClO product scattering is at least an order of magnitude less intense relative to the IO product than is predicted by the "hybrid" statistical complex model. Figure 12 shows the branching ratio as a function of initial reactant translational energy as predicted by the statistical complex model. (These results are from the loose complex model and are taken as the same in the "hybrid" model.) When only the IO product is allowed the exoergic product channel is greatly favored over dissociation of the complex to reform reactants at low collision energies. At high energies the ratios become more nearly equal. As discussed above, this behavior favors scattering at angles near 90°. In contrast, if both product channels are allowed the fraction of complexes dissociating to the IO product remains almost constant with reactant translational energy. For the O + ICl system, only the IO channel can be allowed in order to come close to matching the observed angular distribution. Figure 4 indicates that the experimental data still lies at an angular range too large to be fit by the model. Either some factor that has not been taken into account by the model highly favors reaction at very low collision energies, or some experimental problem such as the presence of van der Waals dimers must account for this.

The behavior shown in Fig. 12 may be qualitatively understood in terms of the number of states available to the dissociating complex in each channel. At low reactant translational energies the energy available to the dissociating complex is dominated by the reaction exoergicity. As more energy is available to the complex, more states become available. Thus, at low collision energies, the more exoergic channel dominates. As the reactant energy increases, the energy available for each channel becomes relatively more nearly equal. Here the density of energy levels comes to dominate. Each channel is simply an atom and a diatomic at the critical configuration. The densities of rotational and vibrational states increase as the rotational constant B_e and the vibrational constant ω_e decrease. The channels giving ICl (reactants), IO and ClO should be favored in that order. In summary, at low reactant translational energy, the more exoergic channel dominates but as the energy increases the channel giving the diatomic molecule with the largest density of energy states begins to dominate.

Both the lack of any observable ClO or BrO product and the position of the IO product angular position indicates that only the IO channel is allowed for these two reactant systems. The most reasonable explanation for this behavior is the geometry of the complex when all three atoms are interacting strongly. This will be discussed fully in the next section.

Both Lee et al[8] and Grice et al[7] have published results for O + ICl scattering at low collision energies and with velocity analysis. The results of Grice et al[7] are very similar to our results while the results of Lee et al[8] who employed an oxygen atom nozzle beam show better resolution in the center-of-mass and show a double peak in the LAB distribution. Our "extra" intensity near the ICl beam may be due to the presence of ICl dimers which could yield such scattering.[42] The velocity results obtained by the other groups have been fit using the RRKM-AM[13] model. Grice et al[7] tentatively interpreted their data

in terms of a loose complex model rather than the tight complex model we have used. Lee et al[8] do not present details of their calculations so we cannot discuss this point in relation to their work. As indicated in Figure 4 here, the angular distribution is better fit by the loose complex calculation at the collision energy that pertains to the experiments reported here.

IO Bond Energy. Two divergent values may be found in the literature for the dissociation energy of the IO molecule: ~44 kcal/mole[43] and ~57 kcal/mole.[44] In this study the reaction of O with ICl (D_0 = 49.6 kcal/mole[36]) to give the product IO has been found to proceed at low collision energies. The reaction of O + CF_3I (D_0 for CF_3-I = 54 kcal/mole[45]) to yield IO + CF_3 is also spontaneous at thermal energies.[46,47] For these two reactions to proceed readily they must be either exoergic or only slightly endoergic, so the reactant bonds broken in these two reactions may be taken as approximate lower limits for the IO dissociation energy. These considerations certainly preclude the 44 kcal/mole value and suggest that the larger value is approximately the minimum value consistent with the results of the O + CF_3I reaction.

The data obtained in this study for the O + ICl reaction provide a sensitive test for the true value of the IO dissociation energy. This dissociation energy is one parameter of the statistical complex models. A value of 57 kcal/mole gave the best overall fit to the angular and velocity distributions. Variations of 2 kcal/mole gave significantly poorer fits. For the O + I_2 and O + IBr reactions the same D_0 value was used in the calculations and gave good results, but since these reactions are more exoergic, the fit is not nearly as sensitive to the value of this parameter. We, thus, suggest a value of 57 $\pm$ 2 kcal/mole for the dissociation energy D_0 of IO. Other molecular beam studies of this reaction[7,8] determined a slightly lower value: 53 $\pm$ 3 kcal/mole. The slight disagreement between the two molecular beam studies is perhaps due to the assumption of a loose collision complex model for the velocity distribution calculations.

Total Reaction Cross Sections. Table III gives Q_c, the total cross section for complex formation predicted by the statistical complex model, and Q_R, the total cross section for reaction, which is obtained from Q_c by multiplying by the branching ratio predicted from the loose collision complex model. The rough experimental values of Q_R obtained in this study are $\sim 10 \text{ A}^{o\,2}$. The pre-exponential factor of the rate constant from the flow tube study of the $O + Cl_2$ reaction[5a] corresponds to $Q_R \sim 1 \text{ A}^{o\,2}$. These experimental values are significantly lower than the model predictions. Such has been the case in other studies[48] of reactions proceeding through long-lived complexes where it has been possible to estimate the magnitude of the total cross section or compare reactive and non-reactive scattering. This behavior is usually interpreted as indicating that a large fraction of the collisions which surmount the centrifugal barrier still cannot form a complex which is capable of dissociating to form products. Grice[7] has suggested that for these reactions only the complexes which form with a nearly collinear O-X-Y orientation are capable of dissociating as products. As will be discussed in the next section, this is in accord with the most stable geometry of the collision complex believed formed in these reactions.

DISCUSSION: ELECTRONIC STRUCTURE

The experimental results demonstrate that the reaction of oxygen atoms with diatomic halogens (excluding F_2) proceed via a long-lived complex or an osculating complex in the case of the Cl_2 reaction. Such long-lived three atom complexes probably have well-depths at least of the order of 20 kcal/mole based on estimates from RRKM theory. The molecules XOX are thought to have a $^1A_1$ ground state with an obtuse bond angle[49] based on the structure of Cl_2O;[50] at first glance, these molecules suggest themselves as viable intermediates. However, one must consider the spin and spatial symmetry constraints placed on the intermediate state by the reactant and product states assuming that the reaction occurs on

a single electronic surface.[51] The correlations for the reaction $O+X_2 \rightarrow OX+X$ are summarized in Table IV. The triplet ground state of the oxygen atom, ^3P_g, requires the reactants to have an overall triplet state and this necessitates the formation of a triplet intermediate unless a spin transition occurs. This spin correlation eliminates the ground sate of X_2O, $^1A_1$, from being the complex sampled by this reaction. For three atoms, AB_2, we need consider only three approaches, $C_{\infty v}$, C_S and C_{2v}. All of the complexes have at least one correlation within the triplet manifold with the reactant states. The product states, due to the presence of two doublets, correlate asymptotically with both singlet and triplet states of the intermediate.

In order to provide further information about the nature of the electronic structure complex, orbital correlations must also be examined.[52] Such correlations are most easily seen for the $C_{\infty v}$ approach of an O atom to the X_2 molecule. This is shown by the "weeny-orbital"[53] diagram in Figure 13. We have ignored the valence s orbital as it is low-lying and will not contribute to the correlations. It is obvious that the $^3\Sigma^-$ state of the intermediate arising from the Π^2 configuration will be repulsive as two "sigma" electrons on the atom are approaching a two electron sigma bond. Thus, for the collinear approach the $^3\Pi$ states of the reactants must correlate with the triplet state of the complex. However, for the intermediate to show the proper correlations, the orbital occupations of the complex must be $\cdots(\pi^*)^3(\sigma^*)^1$ or $\cdots(\sigma^*)^1(\pi^*)^3$ in order to give a $^3\Pi$ state. This is not the $\cdots(\sigma^*)^2(\pi^*)^2$ configuration that we initially predicted[4] and, following us, that Grice predicted,[7] would be the orbital configuration of the complex based simply on state diagrams. Rather this latter configuration gives rise to states that correlate with the repulsive interaction described above. For the C_s approach, a similar correlation can be expected. The orbital correlation diagram for the C_{2v} approach is somewhat more difficult to construct but the correlations can be related to excited states of the molecule X_2O. As shown in

Figure 13, three initial orientations of the O are possible. These orientations correlate with the following triplet states of XOX which we represent by their electron promotions $\pi^* \rightarrow \sigma^*(2)$ and σ-σ^*. The promoted π electron arise from the oxygen not the halogens. We note that one of the states of the $\pi \rightarrow \sigma^*$ type places two electrons in an O atom orbital directed at the σ-bond of X_2. As in the similar case in the $C_{\infty v}$ approach we expect this state to be quite repulsive leading to a high barrier.

Investigation of the experimental evidence on the spectra of OCl_2[54] and the beam results led to the elimination of a C_{2v} geometry describing the intermediate. The absorption spectra for Cl_2O shows continuous absorption suggesting that all excited states lead to dissociation. The spectrum shows a sharp cutoff at 15,000 cm^{-1} (43 kcal/mole) corresponding to the $O+Cl_2$ dissociation limit. No spectral features at lower energies were observed. Although this evidence for the absence of bound excited states is not completely conclusive, it is suggestive of the fact that the accessible C_{2v} geometries are probably too high in energy to be considered as a viable intermediate. Further evidence against the C_{2v} geometry come from our scattering experiments. For the reaction of O with both ICl and IBr only the product IO was observed even though formation of the other product, OCl or OBr respectively, would be more exothermic. Since the reactions proceed via a long-lived complex, the products should be distributed statistically and the more exoergic products would be produced in greater yield if they are accessible geometrically. From the C_{2v} geometry, dissociation to either product would be geometrically feasible and if the C_{2v} geometry was being sampled both products would be observed with the OI being the minor product. However, since we do not observe the other products we can eliminate the C_{2v} geometry from consideration. These results lead us to the conclusion that the geometry of the intermediate is an unsymmetric

triplet of the form OXY with either a linear or bent configuration (we cannot distinguish between these geometries from our results) and an orbital configuration using the $C_{\infty v}$ notation of either $\cdots(\sigma^*)^1(\pi^{*3})$ or $\cdots(\pi^*)^3(\sigma^*)^1$. Further we note for the case where the halogen is unsymmetric, that the intermediate has the halogen with the lowest electronegativity in the central position of the complex. This follows directly from our observation that only OI is produced in the O+ICl and O+IBr reactions.

Our structure for the intermediate shows an interesting feature on the Walsh orbital diagram for these species. Walsh predicted[55] that the upper orbitals in the general diagram are ordered $\cdots\pi,\pi^*;\sigma;\sigma^*$ by increasing energy while Mulliken predicted[56] an ordering $\cdots\pi,\sigma^*;\pi^*;\sigma^*$. For our predicted triplet state with orbital occupancy $\pi^{*3}\sigma^{*1}$ or $\sigma^{*1}\pi^{*3}$ the middle σ^* and π^* orbitals must be essentially degenerate. If they are not degenerate then a π^2 configuration arises if σ^* is lower than π^* while a π^4 configuration arises for π^* lower than σ^*. However, neither of these configurations is allowed as the former arises from a repulsive interaction as discussed previously while a π^4 configuration leads to a singlet state which is not allowed. Since the σ^* and π^* orbitals are predicted to have a strong angular dependence with σ^* increasing rapidly with decreasing angle then it is unlikely that the molecule is strongly bent since this would break the accidental σ^*-π^* degeneracy and lead to incorrect states of the intermediate.

Evidence from other studies supports our conclusions as to the nature of the complex. Rochkind and Pimentel[57] have identified an isomer of Cl_2O in a matrix isolation study of the photolysis of Cl_2O. Using infrared methods, they characterized a species Cl···ClO with the ClO being similar to the diatomic and the remaining Cl being weakly bound to the chlorine of the chatomic. They also suggest that the molecule is not linear and that the bonding between

chlorines follows the model for the (p-π^*)σ bond developed by Spratley and Pimentel.[58] A similar matrix isolation study of FClO has been carried out by Andrews and coworkers.[59] They find a similar structure F···ClO with the F weakly bound to the chlorine end of diatomic ClO with this moiety being very similar to free ClO. The beam results suggested an osculating complex for the O+Cl_2 reaction and we can estimate the stability of the OCl Cl complex as being $\gtrsim$10 kcal/mole. In agreement with these studies an asymmetric form was predicted from the scattering experiments. The second study is in agreement with our prediction that the least electronegative atom (Cl in this case) occupies the central atomic position. For the system OCl Cl it is apparent that the second chlorine polarizes ClO to form a weak bond between the chlorines. For complexes involving heavier halogens, the well depths increase significantly as scattering typical of a long-lived complex is found. Further evidence for the electronegativity ordering of the atoms in the complex comes from studies on the isoelectronic XY_2^+ trihalogen cation where the least electronegative atom is always found to occupy the central site even in the case of Cl_2F^+.[60] These studies always show a bent cation. Similar electronegativity arguments are also found to hold for other reactions of radicals with halogens.[9,11] We note that the O+F_2 reaction has a significant barrier.[6] In this case, the least electronegative element, O, cannot have easy access to the central position (C_{2v} approach) and thus a barrier is expected. It is also likely that the reactions proceeds by a direct mechanism rather than by a complex mechanism. Using the above results, we can summarize our predicted structure for the complex as being an asymmetric triplet OXX with an electron configuration of either $\cdots(\sigma^*)^1(\pi^*)^3$ or $\cdots(\pi^*)^3(\sigma^*)^1$ and most likely the complex is linear or slightly bent.

We now compare these complexes with other known species in order to place them in a chemical perspective. If we replace the O atom, by a halogen the complex has the structure X_3 and is expected to be quite weakly bound as is

found from molecular beam studies[11] of the reaction $X+Y_2$ which showed the presence of osculating complexes. Substitution of a halogen in our complex by an oxygen yields XO_2 which for ClO_2 has two stable isomers[61] OClO and OOCl in doublet states. Indeed the latter asymmetric isomer is predicted to be the more stable form.[62] Substitution of another oxygen leads to ozone which is a ground state singlet with a weak O-O bond. The trend in molecular stabilities for these species follows the addition of extra π^* electrons beginning with ozone. We note that only when there is a full complement of π^* electrons as in X_3 does the system become quite weakly bound. If the species is HX_2 rather than X_3 then there is no complex formed[9] even though the system does follow the electronegativity ordering rule that the least electronegative atom occupies the central site.

Acknowledgements

We gratefully acknowledge support of the early stages of this work by the National Science Foundation and support of its final stages by the Air Force Geophysical Laboratory under contract F19628-78-C-0100.

APPENDIX: MULTI-ANGLE TIME NORMALIZATION FOR ANGULAR DISTRIBUTION MEASUREMENTS

In many molecular beam experiments the scattering intensity at all angles exhibits a systematic variation with time. Usually one reference angle with a relatively noise-free signal is chosen, and its magnitude is periodically measured to follow this time variation. In this study, all the data points are relatively noisy and the measurement of each is repeated several times. Therefore, a more sophisticated time normalization treatment is required. The procedure adopted here[63] is (1) to calculate the most probable value of the mean of all the raw data points taken at each angle, (2) to calculate reduced data points by dividing each data point by the calculated mean of all the data points taken at that angle, (3) to fit all of these reduced data points to a Legendre polynomial expansion in time, (4) to obtain time normalized data points by dividing each original data point by the value of the Legendre expansion corresponding to the time that the data point was taken, and (5) to repeat steps (2) - (4) with the mean recalculated from the time normalized data points obtained in step (4). This iteration continues until the sum of the squares of the deviations of the reduced data points from the Legendre expansion converges to a minimum. It is considered important here to obtain reliable confidence limits on the final results; thus error propagation techniques[64] are used to generate statistically meaningful error bars on the final averaged, time normalized signals. A paragraph will now be devoted to the calculations required for each of the above steps.

A single measurement, S_{ij}, of the reactive scattering at angle j is the difference of the modulated signal with the beam flag open and closed. The modulated signal is the difference between the counts on the "on" scalar, N_A, and the counts on the "off" scalar, N_B:

$$S_{ij} = (N_A - N_B)_{open} - (N_A - N_B)_{closed} \qquad (A1)$$

For each of the four scalar readings in Eq. (A1), the distribution of the magnitudes for an infinite number of measurements of S_{ij} is expected to be a Poisson distribution. Therefore, the standard deviation of the respective distributions may be estimated from a single reading by $\sqrt{N}$. The standard deviation σ_{ij}, of the distribution of S_{ij} values is thus approximated by

$$\sigma_{ij} = [(N_A + N_B)_{open} + (N_A + N_B)_{closed}]^{\frac{1}{2}} \qquad (A2)$$

Ignoring systematic time variations of the scattering intensity for the moment, the most probable value of the mean of the distribution of S_{ij} that may be calculated from the finite number of experimental measurements is given by a weighted mean:[68]

$$S_j = \sum_i (S_{ij}/\sigma_{ij}^2)/\sum_i (1/\sigma_{ij}^2) \qquad (A3)$$

The uncertainty in S_j is given by the estimated standard deviation, σ_j, of the distribution of many determinations of S_j:

$$\sigma_j = [1/\sum_i (1/\sigma_{ij}^2)]^{\frac{1}{2}} \qquad (A4)$$

Now the reduced data points may be calculated:

$$s_{ij} = \frac{S_{ij}}{S_j} \qquad (A5)$$

The uncertainty of each reduced data point, $\bar{\sigma}_{ij}$, must also be calculated:

$$\frac{\bar{\sigma}_{ij}^2}{s_{ij}^2} = \frac{\sigma_{ij}^2}{S_{ij}^2} + \frac{\sigma_j^2}{S_j^2} - \frac{2\sigma_{ij,j}^2}{S_{ij}\, S_j} \qquad (A6)$$

Here $\sigma_{ij,j}$ is the covariance of S_{ij} and S_j, and must be approximately equal to σ_j.

The time normalization function is a weighted least-squares fit of the reduced data points to a Legendre polynomial expansion defined by

$$F(t) = \sum_n a_n P_n (\cos t) \qquad (A7)$$

where $0 \leq t \leq 180$. Each of the reduced data points is weighted by $1/\bar{\sigma}_{ij}^2$. It is necessary to express the time span, T, of the experiment on the range of t. This coordinate change is accomplished by $t=cT-d$ where $c = 0.98\ [180/(T_{max}-T_{min})]$ and $d = c\ T_{min} - (.02)(180)$. A maximum of ten polynomials is used, but the expansion is terminated at a lesser number, m, if two conditions are met. First the F distribution test of an additional term as described in Reference 64 is applied after the calculation of each additional term to determine if that term is statistically justified. If the probability is $\sim$ 5% or greater that a set of points with random deviations from the m term expansion would be fit by the m + 1 term expansion as well as the true data points are actually fit, then the first condition is fulfilled. Second, the χ^2 test of Reference 64 is used to test the overall fit for m terms. If the probability is $\sim$ 5% or greater that the deviations of the s_{ij}'s from the polynominal expansion are as great as would be expected for the deviations of data points with the given uncertainties from the true time normalization function, then the second condition is fulfilled.

The first approximation, S_{ij}', to the time normalized data points may now be calculated

$$S_{ij}' = S_{ij}/F(t) \qquad (A8)$$

The uncertainty of each S_{ij}' is given by σ_{ij}' in

$$\frac{\sigma_{ij}'^2}{S_{ij}'^2} = \frac{\sigma_{ij}^2}{S_{ij}^2} + \frac{\sigma_{F(t)}^2}{F(t)^2} \qquad (A9)$$

where $\sigma_{F(t)}$, the uncertainty in the time normalization function, is given by:

$$\sigma_{F(t)}^2 = \sum_n P_n^2 (\cos t)\, \sigma_{a_n}^2 \qquad \text{(A10)}$$

where σ_{a_n} is the uncertainty in the determination of a_n. Here the covariance of S_{ij} and $F(t)$ is small and has been neglected.

Now these four steps are repeated with the S_j values for Eq. (A5) calculated from the time normalized data points from Eq. (A8) and uncertainties from Eq. (A9) substituted into (A3). Repetition continues until the sum of the squares of the deviations of the reduced data points from F(t) decreases by less than 5% between two successive calculations. For all the data reported here, two repetitions sufficed, and there was negligible difference between the results of the two iterations. Figure 14 shows the calculated F(t) and reduced data points for the experimental run with the most severe time variation.

Figure 15 gives the final time normalized data. The weighted averages from Eq. (A3) over the final time normalized points are considered to be the best values that can be extracted from the original data. Two sets of error bars are shown; each indicates one standard deviation in the determination of S_j. The left set is calculated from Eq. (A4) and the right set is evaluated from the scatter in the individual time normalized data points at each angle. If the left set is systematically smaller than the right set, it indicates that the time normalization function is trying to match the inherent scatter of the data and fewer terms should be used in the Legendre expansion.

References

1. D. G. Truhlar and D. A. Dixon in "Atom-Molecule Collision Theory: A Guide for the Experimentalist", ed. R. B. Bernstein (Plenum Press, New York 1979) C18.

2. N. C. Blais and D. G. Truhlar, J. Chem. Phys. 61, 4186 (1974).

3. a) J. M. Farrar and Y. T. Lee, J. Am. Chem. Soc., 96, 7570 (1974); b) J. Chem Phys., 63, 3639 (1975); c) J. J. Valentini, M. J. Coggiola, and Y. T. Lee, J. Am. Chem. Soc., 98, 853 (1976); d) Faraday Discuss. Chem. Soc. 62, 232 (1977).

4. Preliminary results have previously been reported: a) D. D. Parrish and D. R. Herschbach, J. Am. Chem. Soc. 95, 6133 (1973); b) D. A. Dixon, D. D. Parrish and D. R. Herschbach, Faraday Discuss. Chem. Soc. 55, 385 (1973)

5. a) M.A.A. Clyne and J. A. Coxon, Trans. Faraday Soc. 62, 2175 (1966); b) H. Niki and B. Weinstock, J. Chem. Phys., 47, 3249 (1967); c) J. N. Bradley, D. A. Whytock and T. A. Zaleski, J. Chem. Soc., Faraday Trans. I. 69, 1251 (1973); d) M. Kaufman and C. E. Kolb, Chem. Instrum. 3, 175 (1971).

6. R. H. Krech, G. J. Diebold and D. L. McFadden, J. Am. Chem. Soc., 99, 4605 (1977).

7. a) C. F. Carter, M R. Levy, K. B. Woodall and R. Grice, Faraday Discuss. Chem. Soc. 55, 381 (1973); b) D.St.A.G. Radlein, J. C. Whitehead and R. Grice, Nature, 253, 37 (1975); c) Mol. Phys., 29, 1813 (1975); d) P. A. Garry, C. V. Nouikow and R. Grice, Chem. Phys. Lett., 49, 116 (1977); e) ibid., 55, 19 (1978).

8. S. J. Sibener, R. J. Buss and Y. T. Lee, XI International Symposium on Rarefied Gas Dynamics 1978 to be published.

9. J. D. McDonald, P. R. LeBreton, Y. T. Lee and D. R. Herschbach, J. Chem. Phys., 56, 769 (1972)

10. a) J. A. Logan, C. A. Mims, G. W. Stewart and J. Ross, J. Chem. Phys., 64, 1804 (1976); b) C. F. Carter, M. R. Levy, and R. Grice, Faraday Discuss. Chem. Soc., 55, 357 (1973).

11. a) J. J. Valentini, Y. T. Lee and D. J. Auerbach, J. Chem. Phys., 67, 4866 (1977); b) Y. T. Lee, P. R. LeBreton, J. D. McDonald and D. R. Herschbach, J. Chem. Phys., 51, 455 (1969); c) N. C. Blais and J. B. Cross, J. Chem. Phys., 52, 3580 (1970); d) D. Beek, F. Engelke and H. J. Loesch. Ber. Bunsenges, Phys. Chem. 72, 1105 (1968).

12. For a review see: D. R. Herschbach, Adv. Chem. Phys. 10, 319 (1966).

13. S. A. Safron, N. D. Weinstein, D. R. Herschbach, and J. C. Tully, Chem. Phys. Lett., 12, 564 (1972).

14. a) O. K. Rice, "Statistical Mechanics, Thermodynamics, and Kinetics", W. A. Freeman, San Francisco, Calif., 1967, pp. 495-573; b) R. A. Marcus, J. Chem. Phys., 43. 2658 (1965); c) P. J. Robinson and K. A. Holbrook, "Unimolecular Reactions", (Wiley-Interscience, London, 1972).

15. D. A. Case and D. R. Herschbach, J. Chem. Phys., 64, 4212 (1976).

16. D. D. Parrish, to be published.

17. Y. T. Lee, J. D. McDonald, P. R. LeBreton, and D. R. Herschbach, Rev. Sci. Instrum., 40, 1402 (1969).

18. J. D. McDonald, Ph.D. thesis, Harvard University, 1971.

19. F. C. Fehsenfeld, K. M. Evenson, and H. P. Broida, Rev. Sci. Instr., 36, 294 (1965).

20. S. V. Filseth, F. Stuhl, and K. H. Welge, J. Chem. Phys., 52, 239 (1970).

21. J. B. Anderson in "Molecular Beams and Low Density Gas Dynamics", (Marcel Dekker, New York, 1974) p. 1.

22. a) W. B. Miller, S. A. Safron and D. R. Herschbach, Discuss. Faraday Soc., 44, 108 (1967); b) G. M. McClelland and D. R. Herschbach, J. Phys. Chem. in press (1979).

23. J. H. Birely, R. R. Herm, K. R. Wilson, and D. R. Herschbach, J. Chem. Phys., 47, 993 (1967).

24. J. C. Light, Faraday Discuss. Chem. Soc., 44, 14 (1967) and work cited therein.

25. See, for example, R. B. Leachman and E. E. Sonmann, Ann. Phys. 18, 274 (1962).

26. S. J. Riley and D. R. Herschbach, J. Chem. Phys., 58, 27 (1973).

27. W. B. Miller, Ph.D. Thesis, Harvard Univ., 1969.

28. For the O + Cl_2, Br_2, and I_2 reactions the product channel was assumed to be doubly degenerate, ^{2} while ^{2} for the mixed halogen reactions, each channel was taken as non-degenerate.

29. H. L. Kramer and D. R. Herschbach, J. Chem. Phys., 53, 2792 (1970).

30. A. I. Vogel, J. Chem. Soc., 644 (1948).

31. R. R. Teachout and R. T. Pack, Atomic Data, 3, 195 (1971).

32. E. Herbst and W. Steinmetz, J. Chem. Phys., 56, 5342 (1972).

33. The IBr Dipole moment is an estimate obtained by considering the relative electronegativities.

34. C. R. Byfleet, A. Carrington, and D. K. Russell, Molec. Phys., 20, 271 (1971).

35. D. deB. Darwent, "Bond Dissociation Energies in Simple Molecules", Nat. Bur. Stand. Pub. NSRDS-NBS 31 (1970).

36. B. Rosen, "Spectroscopic Data Relative to Diatomic Molecules", (Pergamon, New York, 1970).

37. Trial calculations including averaging over the halogen beam velocity indicates it is indeed negligible. The single velocity is taken as the most probable velocity in a nozzle beam with high Mach number assuming complete rotational relaxation and no vibrational relaxation. Thus, $V_2 = 7/2\ d$ where α is the most probable velocity in the gas before the expansion. Velocity analysis of the nozzle beam is consistent with this assumption.

38. The velocities selected were integral multiples of 1/4 α. This covers the full range of velocities present to a significant proportion in a thermal beam.

39. The disagreement in magnitude of the model calculations with the velocity spectra data is deemed to be an experimental problen in the normalization of the velocity distribution to the angular distribution.

40. The work described in Reference 7a-7c employed an O atom beam characterized by a temperature of 350°k.

41. G. A. Fisk, J. D. McDonald and D. R. Herschbach, Discuss. Faraday Soc. 44, 228 (1967).

42. a) D. L. King, D. A. Dixon and D. R. Herschbach, J. Am. Chem. Soc., 96, 3328 (1974); b) D. A. Dixon and D. R. Herschbach, J. Am. Chem. Soc., 97, 6268 (1975); c) D. A. Dixon, Ph.D. Thesis, Harvard U. (1975).

43. E. H. Coleman, A. G. Gaydon, and W. M. Vaidya, Nature, 162, 108 (1948); V. M. Trivedi and V. B. Gohel, J. Phys. B., 5, L38 (1972); M. L. P. Rao, D. V. K. Rao and P. T. Rao, Phys. Lett., 50A, 341 (1974).

44. L. F. Phillips and T. M. Sugden, Trans. Faraday Soc., 57, 914 (1961); R. B. Singh and D. K. Rai, J. Quant. Spect. Rad. Trans., 5, 723 (1965).

45. Lord, Goy and Pritchard, J. Phys. Chem., 71, 2705 (1967).

46. M. Kaufman and C. E. Kolb, Chem. Instrumentation 3, 175 (1971).

47. P. A. Gorry, C. V. Nowikow and R. Grice, Chem. Phys. Lett., 55, 24 (1978).

48. W. B. Miller, S. A. Safron and D. R. Herschbach, J. Chem. Phys., 56, 3581 (1972).

49. B. J. Brisdon in "Inorganic Chemistry, MTP International Review of Science, Series 1, Vol. 3" ed. V. Gutmann (Butterworths, London, 1971) Chap. 8.

50. G. E. Herberich, R. H. Jackson and D. J. Millen, J. Chem. Soc. A, 336 (1966).

51. B. H. Mahan, Accts. Chem. Res. 8, 55 (1975).

52. R. B. Woodward and R. Hoffman, "The Conservation of Orbital Symmetry", (Verlag Chemie, GmbH, Weinheim, 1970).

53. W. A. Goddard, III, J. Am. Chem. Soc., 94, 793 (1972).

54. a) W. Finkelnburg, H-J. Schumacher and G. Steiger, Z. Phys. Chem. B15, 127 (1931); b) M.C.F. Goodeve and J. I. Wallace, Trans. Far. Soc. 26, 254 (1931); c) M. Bodenstein and G. B. Kistiakowsky, Z. Phys. Chem. 116, 371 (1925).

55. A. D. Walsh, J. Chem. Soc.,2266 (1952).

56. R. S. Mulleken, J. Chem. Phys. 3, 739 (1935).

57. M. M. Rochkind and G. C. Pimentel, J. Chem. Phys. 46, 4481 (1967).

58. R. D. Spratley and G. C. Pimentel, J. Am. Chem. Soc., 88, 2394 (1966).

59. L. Andrews, F. K. Chi and A. Avkell, J. Am. Chem. Soc., 96, 1997 (1974).

60. R. J. Gillespie and M. J. Morton in "Inorganic Chemistry, MTP International Review of Science, Series 1, Vol. 3", ed. V. Gutmann (Butterworths, London, 1971) Chapter 7.

61. See reference 48 for a review of this work.

62. J. L. Gole, (unpublished results). Ab initio SCF-CI Calculations Predict the ClOO Isomer to be More Stable.

63. This procedure closely parallels that described in detail elsewhere (D.D. Parrish, Ph.D. thesis, University of California, Berkeley, 1970).

64. See, for example, P. R. Bevington, Data Reduction and Error Analysis for the Physical Sciences (McGraw-Hill Book Co., New York, 1969).

65. Equation (3) is strictly true only for a Gaussian distribution, but since the values of N are large ($\sim 10^3 - 10^5$), the Poisson distributions are closely approximated by Gaussian distributions.

FIGURE CAPTIONS

Figure 1 Schematic of experimental configuration. The components shown are surrounded by a large liquid nitrogen cooled shield and enclosed in a large vacuum chamber. The reactant beams cross at an angle of 90°. Scattered molecules can be observed over the range $\theta = -15^{\circ}$ to 119° in the plane of the incident beams.

Figure 2 Schematic diagrams of beam sources. a) Microwave discharge source for oxygen atom beam, b) Halogen molecule nozzle beam source.

Figure 3 Laboratory angular distributions (number density) of reactively scattered products. The circles indicate the weighted averages of all data taken at each angle; the error bars indicate one standard deviation (see the Appendix for complete discussion.) The $O + Cl_2$ data are an average of two experimental runs. The scattering angle is in the plane of the parent beams. The direction of the O atom beam is at 0°, the halogen beam at 90°. The vertical arrows indicate the position of the centroid velocity vector calculated for the combination of beam velocities of the most probable collision energy. Curves show distributions calculated from collision complex models using the loose (solid curves) or tight linear (dashed curves) transition state models. An approximate calculation for $O + Cl_2$ assuming an activation energy of 2.9 kcal/mole is also included (dot-dash curve).

Figure 4 Laboratory angular distributions of reactively scattered products. Curves and symbols are defined in Fig. 3.

Figure 5 Laboratory angular distributions of reactively scattered products from the O + ICl reaction. The data points indicate the search for the ClO product. Curves indicate the expected ClO product (solid curve) compared to the IO product (dashed curve) as predicted by the loose transition-state model. Equal detection efficiencies for the two products were assumed to normalize the curves and data points.

Figure 6 Laboratory velocity spectrum (flux density) of reactively scattered ClO product at a scattering angle of 60^{o} for the O + Cl_2 reaction. The error bars indicate one standard deviation and include the uncertainty in the normalization to the angular data as well as that in the velocity spectra measurement. The vertical arrow indicates the upper limits on the velocity from energy conservation for the nominal collision energy. Curves show distributions calculated from the statistical complex models convoluted over the velocity resolution of the detector. The solid curve is for a loose complex; the other two are for a tight linear complex; the dot-dash curve includes an approximate treatment for an activation energy of 2.9 kcal/mole.

Figure 7 Laboratory velocity spectra of reactively scattered BrO product at indicated scattering angles for the O + Br_2 reaction. The curves (as in Fig. 6) are calculated from the statistical complex models; here convolution over the velocity resolution of the detector was not necessary.

Figure 8 Laboratory velocity spectra of reactively scattered IO product at indicated scattering angles for the O + ICl reaction. The curves

(as in Figure 6) are calculated from the statistical complex models with no convolution over the velocity resolution of the detector. The three horizontal bars indicate this velocity resolution (FWHM) at the respective velocities.

Figure 9 Polar (velocity-angle) contour map of BrO reactively scattered flux intensity in the center of mass system. The O atom beam direction is 0° and that of the halogen molecule beam is 180°. Ticks along the radial lines mark velocity increments of 100 m/sec.

Figure 10 Product distributions in the CM system for the O + Br_2 reaction. Experimental curves (solid lines) were derived from Figure 9. The results of the loose (dashed) and tight-linear (dot-dash) transition-state models are shown. The angular distributions (a) are each normalized so that the total scattering given by $2\pi \int_0^{\pi} I(\theta) \sin \theta d\theta$ is equal to unity. Included in (a) is the curve (dotted) expected if orbital angular momentum dominates. The velocity distributions (b) and the corresponding relative translational energy distributions (c) are all normalized so that their total integrals equal unity.

Figure 11 (a) CM angular distributions calculated from the loose transition-state model. The curves have been arbitrarily normalized to 1.0 at $\theta = 0^{\circ}$. The θ range 90° - 180° is a reflection about 90° of the 0° - 90° range. (b) Product translational energy distributions calculated from the tight linear transiton state model. For clarity the curves for the O + ICl and O + IBr reactions have been lowered by one unit along the ordinate. The curves are normalized so that their integral is equal to unity.

Figure 12 Probability of complex decomposition to each channel as a function of initial translational energy for the O + ICl reaction. Dashed curves pertain to when the I + ClO channel is forbidden, solid curves to when all three channels are allowed.

Figure 13 Orbital correlation diagram for the C_{2v} and $C_{\infty v}$ approaches of an O atom (^3P_g) to a diatomic homonuclear halogen a) C_s approach. The state symmetry is shown on the left while the orbital configurations of the complex are shown on the right. Note the repulsive interaction for the $^3\Sigma^-$ approach. b) C_{2v} approach. The notation for the excitation corresponds to the type of orbital excited from, in this case a σ bonding orbital or a π out-of-plane orbital, to an anti-bonding σ^*. We have not tried to identify which orbital is the σ or π orbitals, but presumably they are the $6a_1$ and $2b_1$ orbitals respectively. The σ^* orbitals would be expected to be the $7a_1$ and $5b_2$ orbitals. Note the repulsive interaction in diagram on the right.

Figure 14 Time normalization function and reduced data points for the O + I_2 reaction data presented in Figure 3. Each reduced data point is obtained by dividing an individual measurement of the signal at a given angle by the mean of all the measurements made at that angle. The abscissa scale is obtained by linearly normalizing the time span of the experiment to a 0 to 180 span for purposes of the Legendre polynomial expansion. At t = 40, the O beam discharge source was retuned resulting in a sharp increase in product scattering intensity.

Figure 15 Time normalized data points (open circles) and weighted averages (solid diamonds) for data of Fig. 14. The error bars indicate two-thirds confidence limits (one standard deviation) for the determination of the average. The left bars are calculated by the error propagation techniques discussed in the text, and the right bars are evaluated from the scatter in the individual data points shown.

TABLE I. PARENT BEAM PARAMETERS[a]

Reactant	T_0	T_N	P_N
Cl_2	1200	683	400
Br_2	1000	473	870
I_2	1200	473	150
ICl	1200	418	260
IBr	1200	402	160

[a] T_0 and T_N denote the temperatures (^oK) of the oxygen atom beam and nozzle source respectively. T_0 was determined by velocity analyzing the oxygen atom beam under identical conditions and fitting the results to a Maxwell-Boltzmann velocity distribution to extract the temperature. P_N refers to the halogen gas pressure (torr) behind the nozzle; this pressure is determined from the vapor pressure of the halogen at the temperature of the supply reservoir except for Cl_2 for which the pressure was approximately measured by a gauge.

TABLE II. PARAMETERS FOR TRANSITION-STATE MODELS[a]

Parameter	O + Cl_2	O + Br_2	O + I_2	O + ICl	O + IBr
$C(10^{-12}$ erg.Å^6)	96	117	165	135	142
$C'(10^{-12}$erg.Å^6)	173	258	541	281 309	351 375
W(kcal/mole)	1.0	0.7	0.9	0.6	0.6
D_o XY(kcal/mole)	57.2	45.4	35.6	49.6	41.9
D_o XO(kcal/mole)	63.3	55.3	57	57 63.3	57 55.3
E_{COLL}(kcal/mole)[b]	3.92	2.11	2.44	2.43	2.41
ω_e XY(cm^{-1})	559.7	323.3	214.5	384.3	268.7
ω_e XO(cm^{-1})	780	771	681.4	681.4 780	681.4 771
B_e XY(cm^{-1})	0.2441	0.0811	0.0374	0.1141	0.0561
B_e XO(cm^{-1})	0.622	0.4278	0.3403	0.3403 0.622	0.3403 0.4278

[a]For the quantities where two entries are given for the mixed halogen reactions, the upper value is for the IO product channel and the lower value is for the alternate (ClO or BrO) product channel.

[b]Initial collision energy

TABLE III. CROSS SECTIONS CALCULATED FROM LOOSE TRANSITION STATE MODEL[a]

Reaction	$Q_C(\text{Å}^2)$	$Q_R(\text{Å}^2)$
$O + Cl_2$	42	35
$O + Br_2$	55	45
$O + I_2$	59	50
$O + ICl$	55	42
$O + IBr$	56	43

[a]The quantity Q_c is calculated from Eq. (13) of text at the nominal collision energy. Q_R is obtained by multiplying Q_c by the branching ratios predicted from the loose complex model averaged over reactant translational energy. Only the IO channel was allowed in the mixed halogen reactions.

TABLE IV. STATE CORRELATIONS FOR $O+X_2$ REACTIONS

Approach Geometry	Reactants $[O(^3P_g)+X_2(^1\Sigma_g^+)]$	Intermediate (Possible)	Products $[X(^2P_u)+OX(^2\pi)]$
$C_{\infty v}$	$^3\Sigma^- + {}^3\pi$	$^1\Sigma^+ + {}^3\Sigma^- + {}^1\Delta$ [a] $+ {}^1\Sigma^+$ [b] $+ {}^3\pi + {}^1\pi$ [c]	$^3\Delta + {}^3\pi + {}^3\Sigma^+ + {}^3\Sigma^-$ $+ {}^1\Delta + {}^1\pi + {}^1\Sigma^+ + {}^1\Sigma^-$
C_s	$2(^3A') + {}^3A''$	$^1A' + {}^1A'' + {}^3A' + {}^3A''$ [d]	$3(^3A') + 3(^3A'')$ $+3('A') + 3('A'')$
C_{2v}	$^3A_2 + {}^3B_1 + {}^3B_2$	$^1A_1$ [e] $+ {}^3A_1 + {}^3B_1 + {}^3B_2$ [f] $+ {}^1A_1 + {}^1B_1 + {}^1B_2$ [f]	$2(^3A_1) + 2(^3A_2) + {}^3B_1 + {}^3B_2$ $+2(^1A_1) + 2(^1A_2) + {}^1B_1 + {}^1B_2$

[a] These states arise from the $\cdots(\sigma^*)^2(\pi^*)^2$ electron configuration.

[b] This state arises from the $\cdots(\pi^*)^4$ electron configuration.

[c] These states arise from either the $\cdots\cdot(\pi^*)^3(\sigma^*)^1$ or $\cdots(\sigma^*)^1(\pi^*)^3$ electron configurations. The singlet states of the $C_{\infty v}$ intermediate could arise from the $O(^1D_g)$ excited state which gives $^1\Sigma^+ + {}^1\pi + {}^1\Delta$.

[d] These states arise from the $\cdots(a')^2$, $\cdots(a'')^2$ or $\cdots(a')^1(a'')^1$ configurations.

[e] This state arises from the ground state configuration.

[f] These states arise from the confgurations $\cdots\cdot(b_1)^1(a_1)^1$, $\cdots(a_1)^1(a_1)^1$ and $\cdots(b_2)^1(a_1)^1$ estimated from Walsh diagrams.

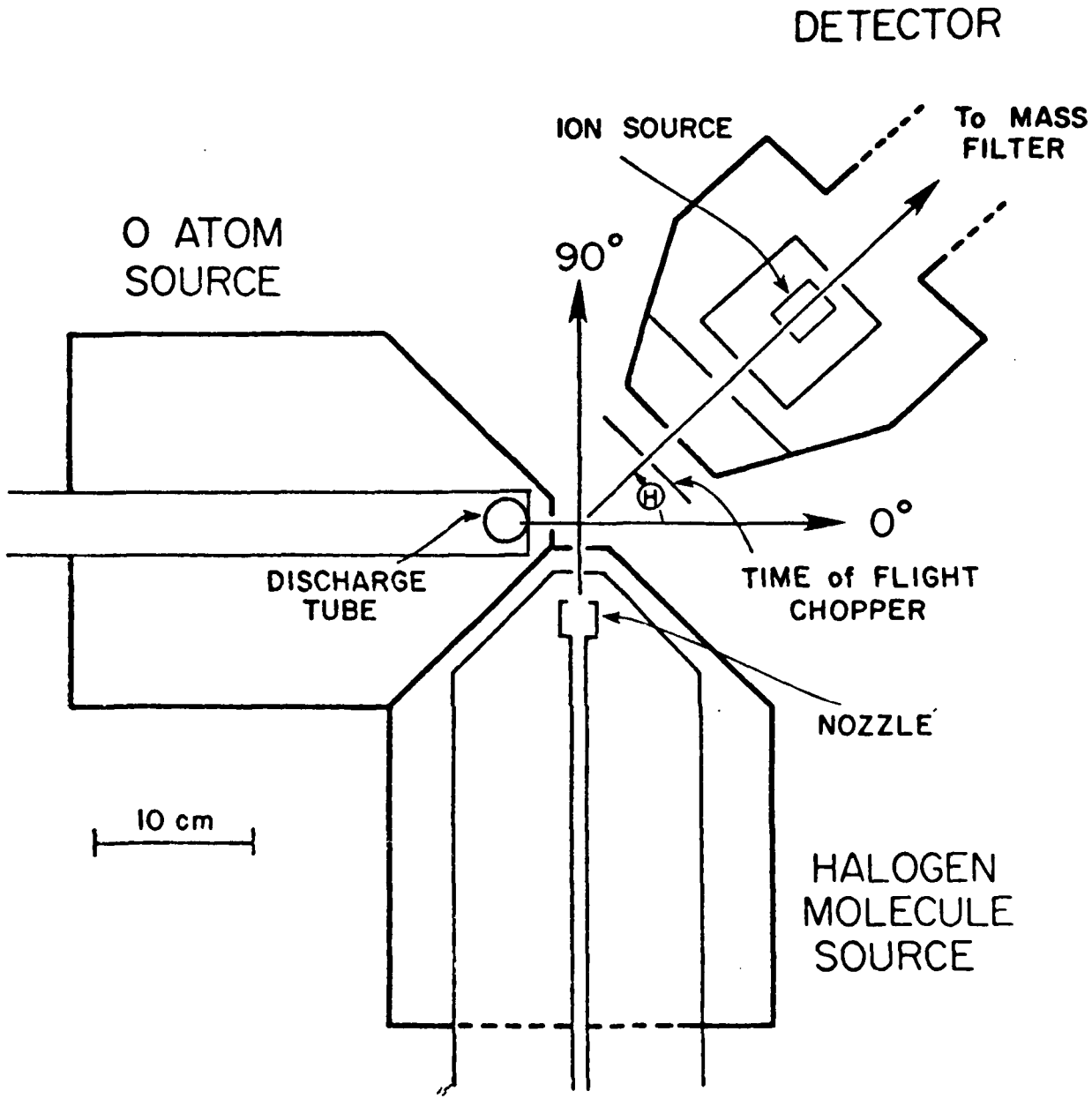
DETECTOR
ION SOURCE
To MASS FILTER
O ATOM SOURCE
90°
0°
DISCHARGE TUBE
TIME of FLIGHT CHOPPER
NOZZLE
10 cm
HALOGEN MOLECULE SOURCE

FIGURE 1

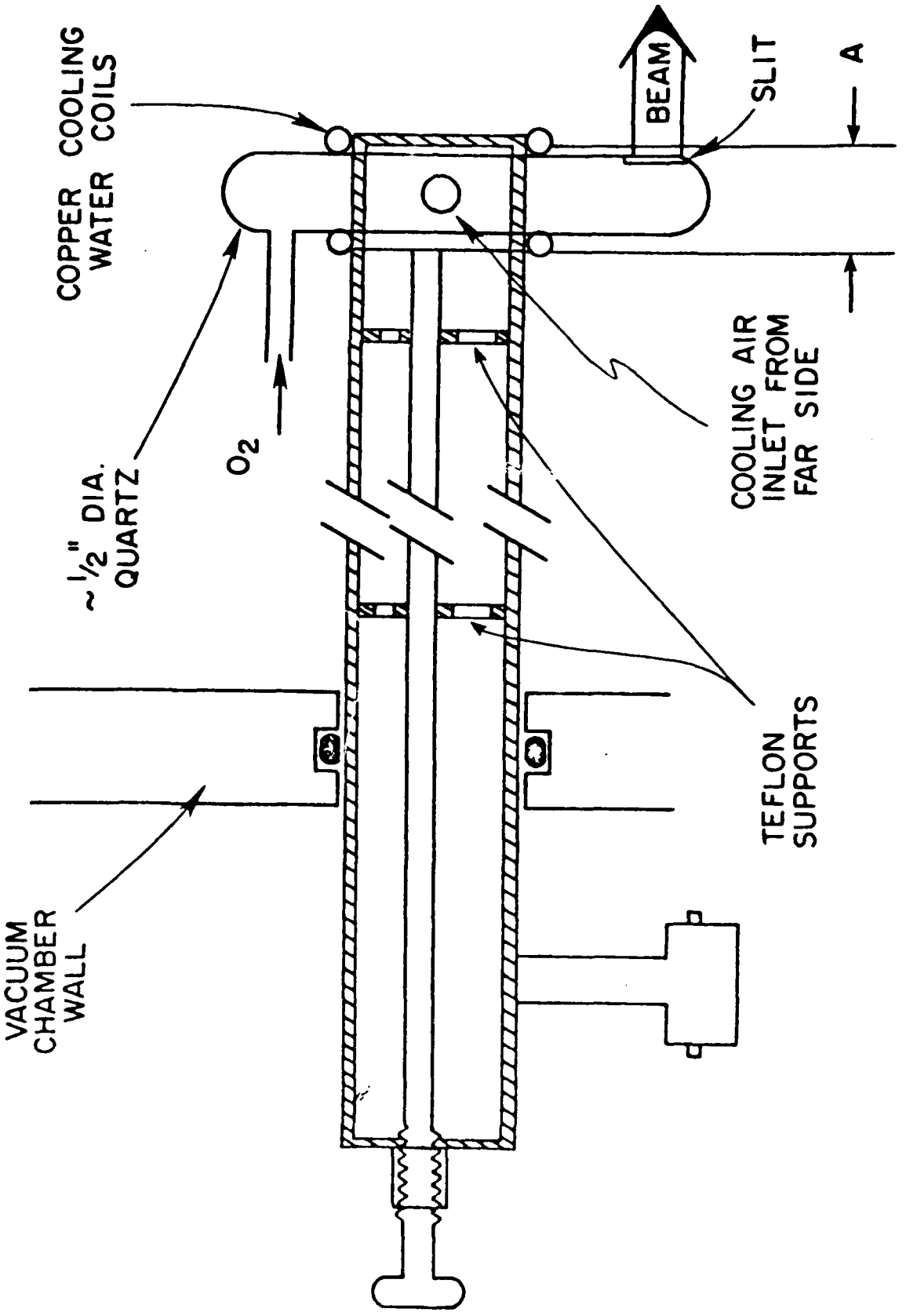
COPPER COOLING WATER COILS
BEAM
SLIT
A
~½" DIA. QUARTZ
O2
COOLING AIR INLET FROM FAR SIDE
TEFLON SUPPORTS
VACUUM CHAMBER WALL

FIGURE 2(A)

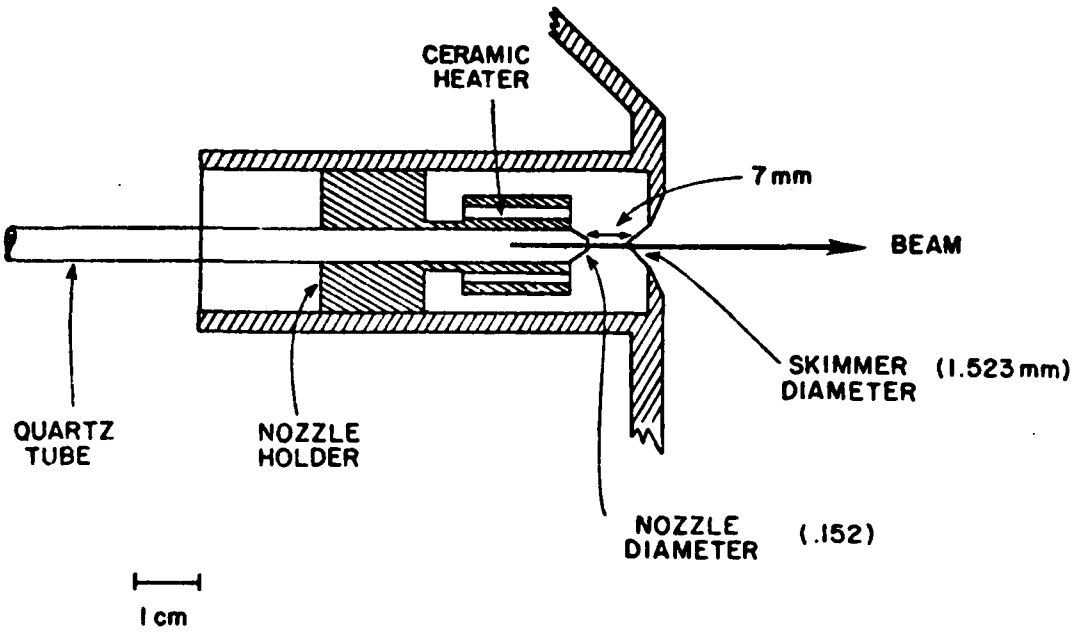
CERAMIC
HEATER
7 mm
BEAM
SKIMMER (1.523 mm)
DIAMETER
QUARTZ
TUBE
NOZZLE
HOLDER
NOZZLE
DIAMETER (.152)
1 cm

FIGURE 2(B)

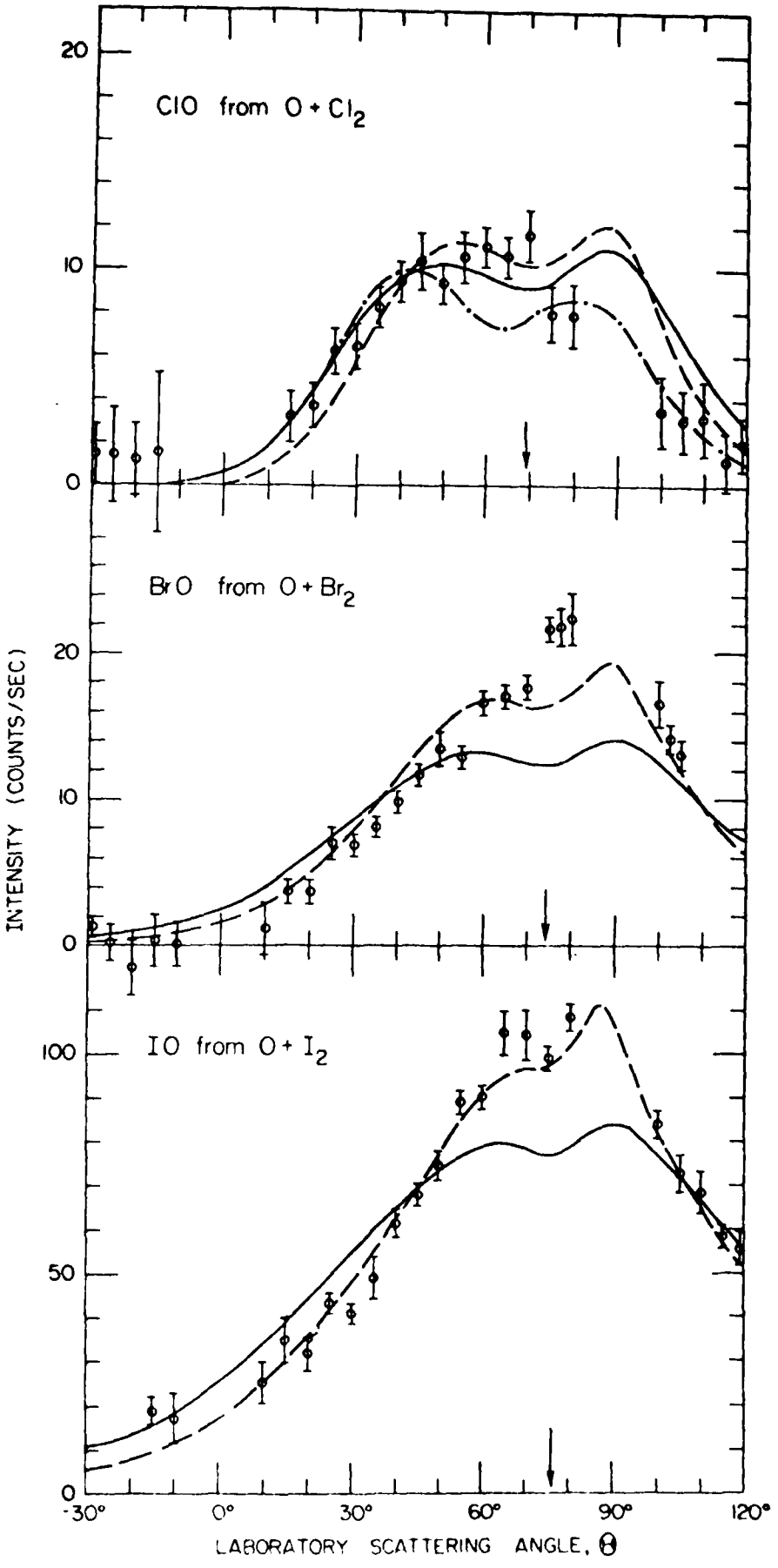
ClO from O + Cl2
BrO from O + Br2
IO from O + I2
INTENSITY (COUNTS/SEC)
LABORATORY SCATTERING ANGLE, Θ
20
10
0
20
10
0
100
50
0
-30°
0°
30°
60°
90°
120°

FIGURE 3

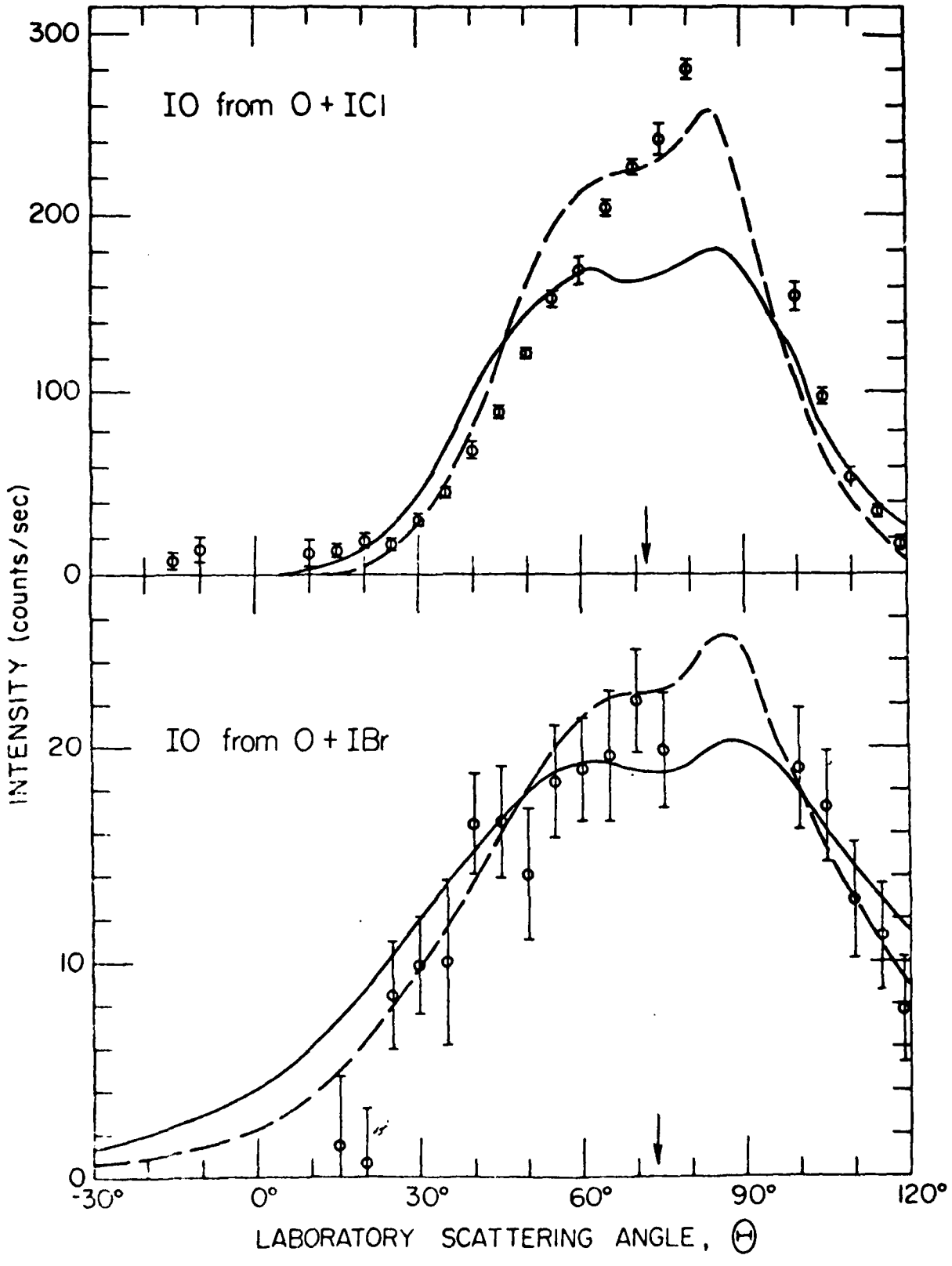
IO from O + ICl
IO from O + IBr
INTENSITY (counts/sec)
300
200
100
0
20
10
0
-30°
0°
30°
60°
90°
120°
LABORATORY SCATTERING ANGLE, Θ

FIGURE 4

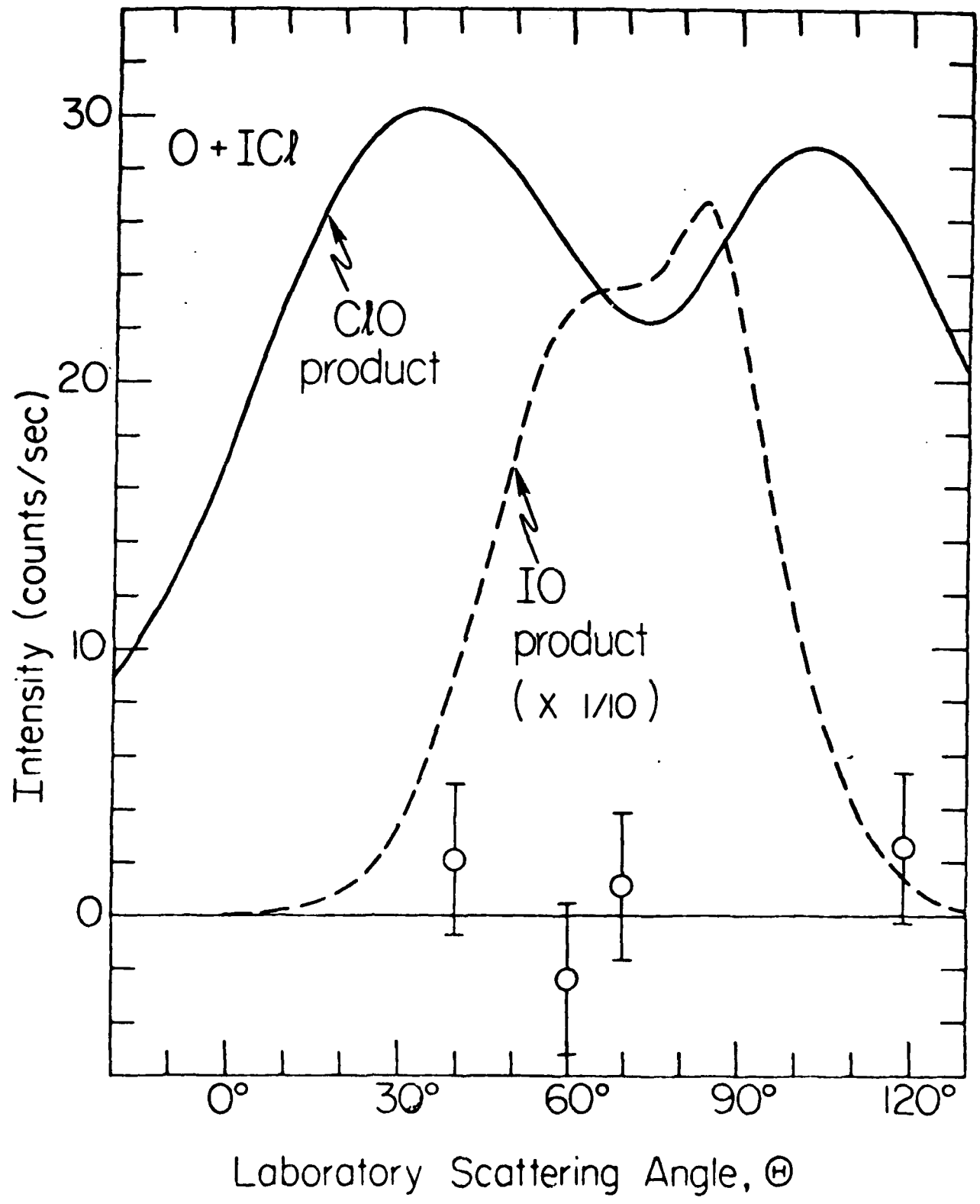
O + ICl
ClO
product
IO
product
(x 1/10)
Intensity (counts/sec)
30
20
10
0
0°
30°
60°
90°
120°
Laboratory Scattering Angle, Θ

FIGURE 5

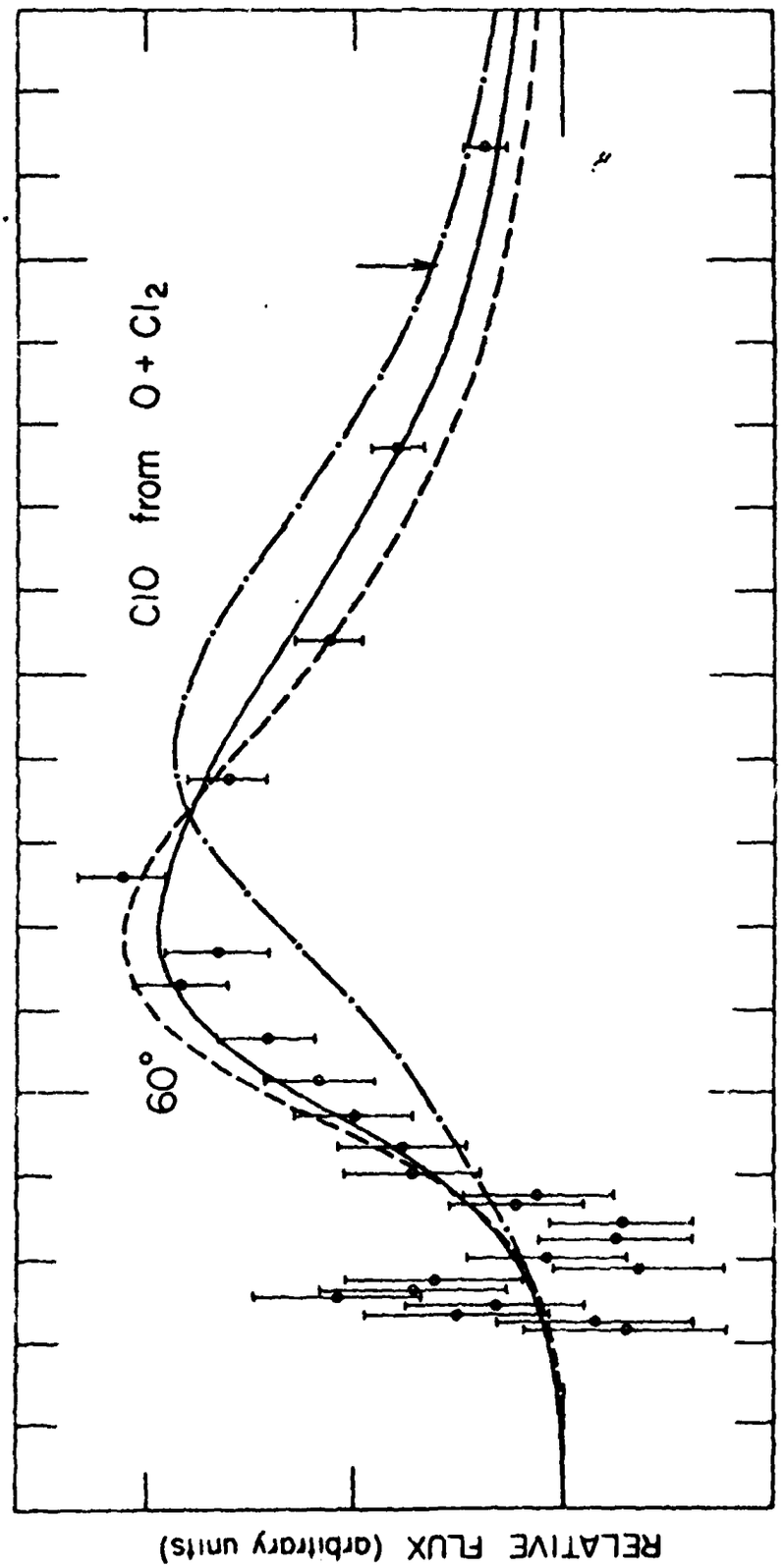
ClO from O + Cl2
60°
500
1000
1500
LABORATORY VELOCITY (m/sec)
RELATIVE FLUX (arbitrary units)

FIGURE 6

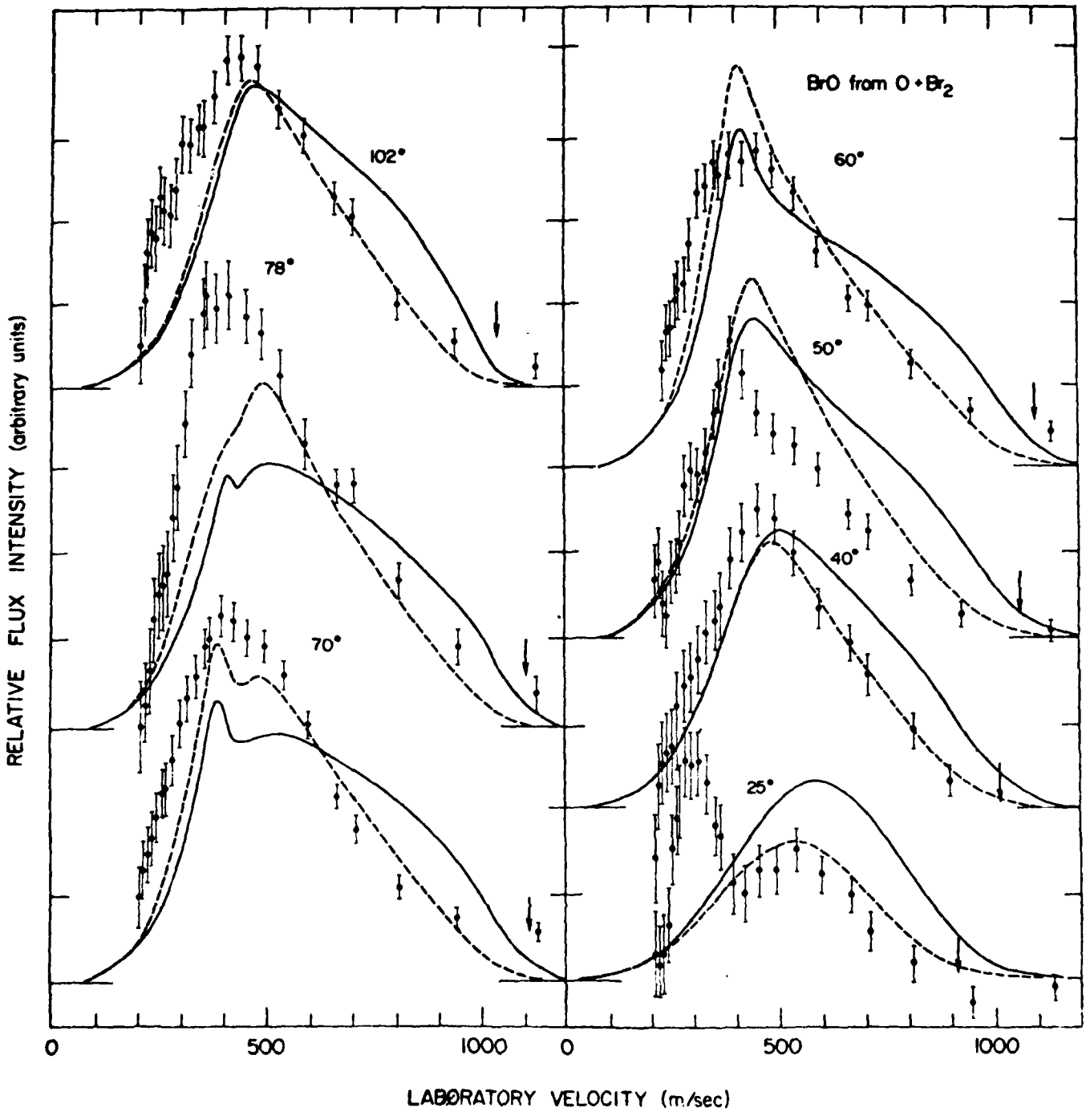
BrO from O + Br2
102°
78°
70°
60°
50°
40°
25°
RELATIVE FLUX INTENSITY (arbitrary units)
0
500
1000
0
500
1000
LABORATORY VELOCITY (m/sec)

FIGURE 7

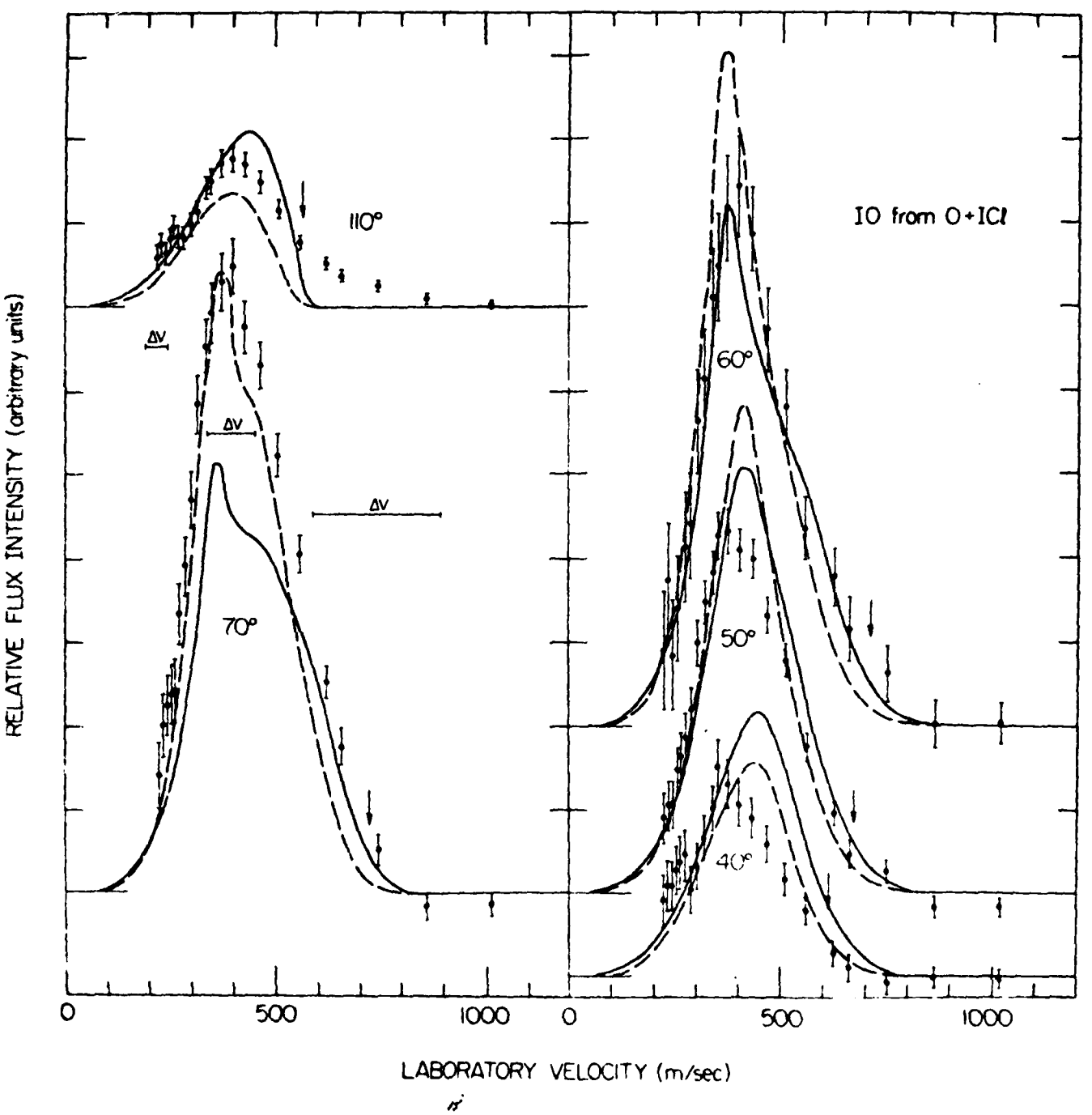
IO from O+ICl
110°
70°
60°
50°
40°
ΔV
ΔV
ΔV
RELATIVE FLUX INTENSITY (arbitrary units)
0
500
1000
0
500
1000
LABORATORY VELOCITY (m/sec)

FIGURE 8

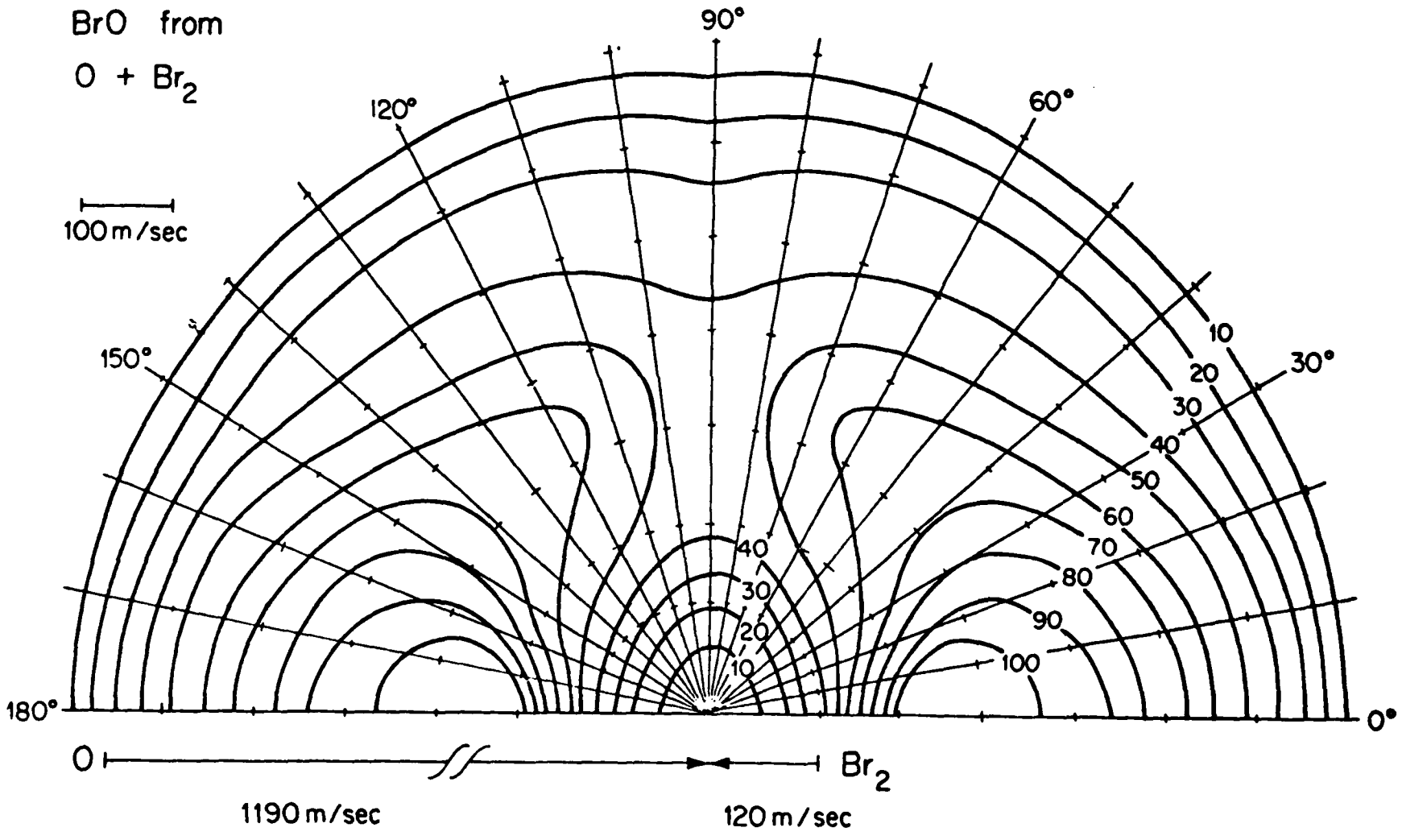
BrO from
O + Br2
90°
120°
60°
150°
30°
180°
0°
100 m/sec
10
20
30
40
50
60
70
80
90
100
40
30
20
10
O
Br2
1190 m/sec
120 m/sec

FIGURE 9

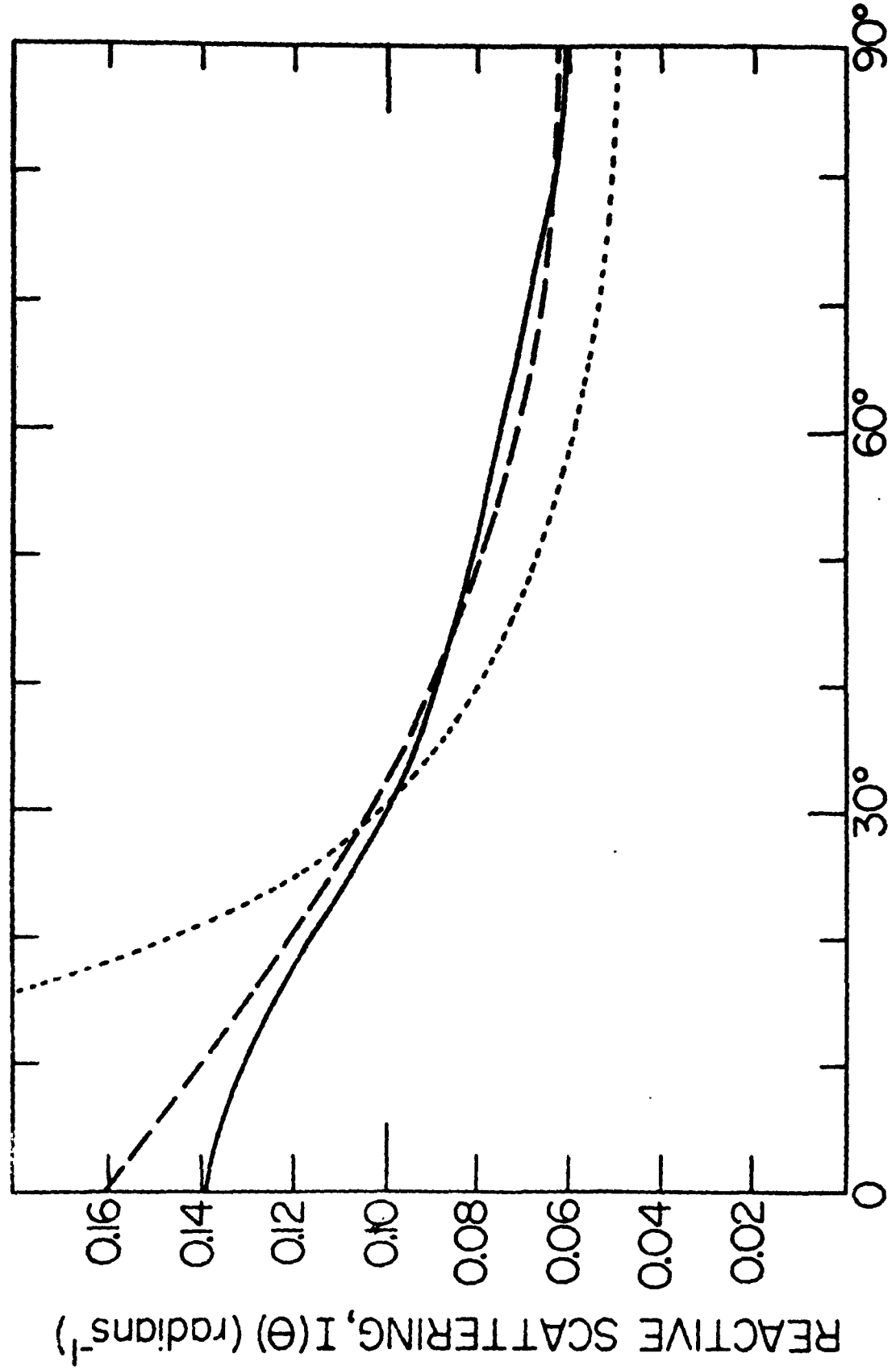
REACTIVE SCATTERING, I(Θ) (radians⁻¹)
0.16
0.14
0.12
0.10
0.08
0.06
0.04
0.02
0
30°
60°
90°
CM SCATTERING ANGLE, Θ

FIGURE 10(A)

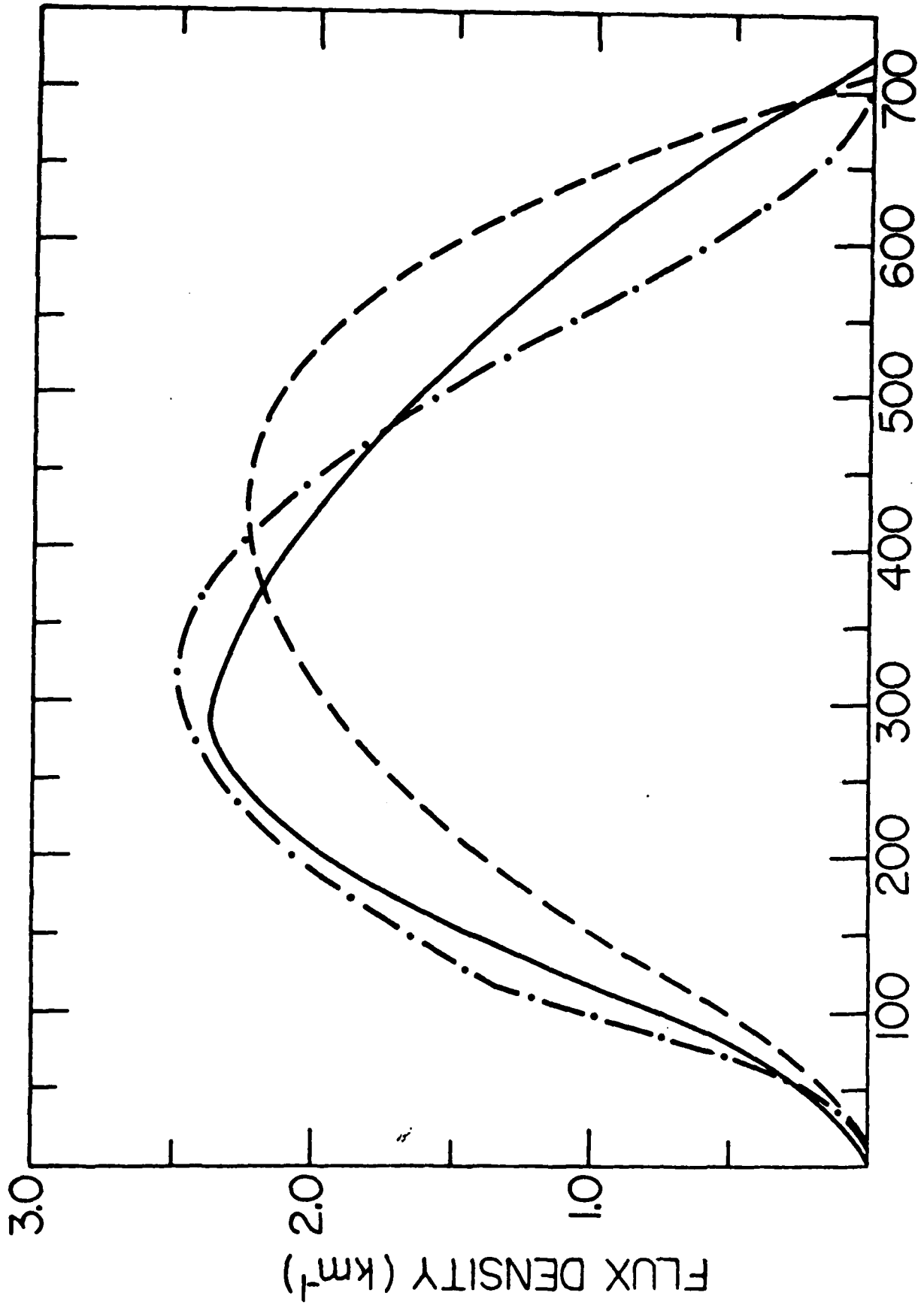
FLUX DENSITY (km⁻¹)
3.0
2.0
1.0
100
200
300
400
500
600
700
CM RECOIL VELOCITY u(m/sec)

FIGURE 10(B)

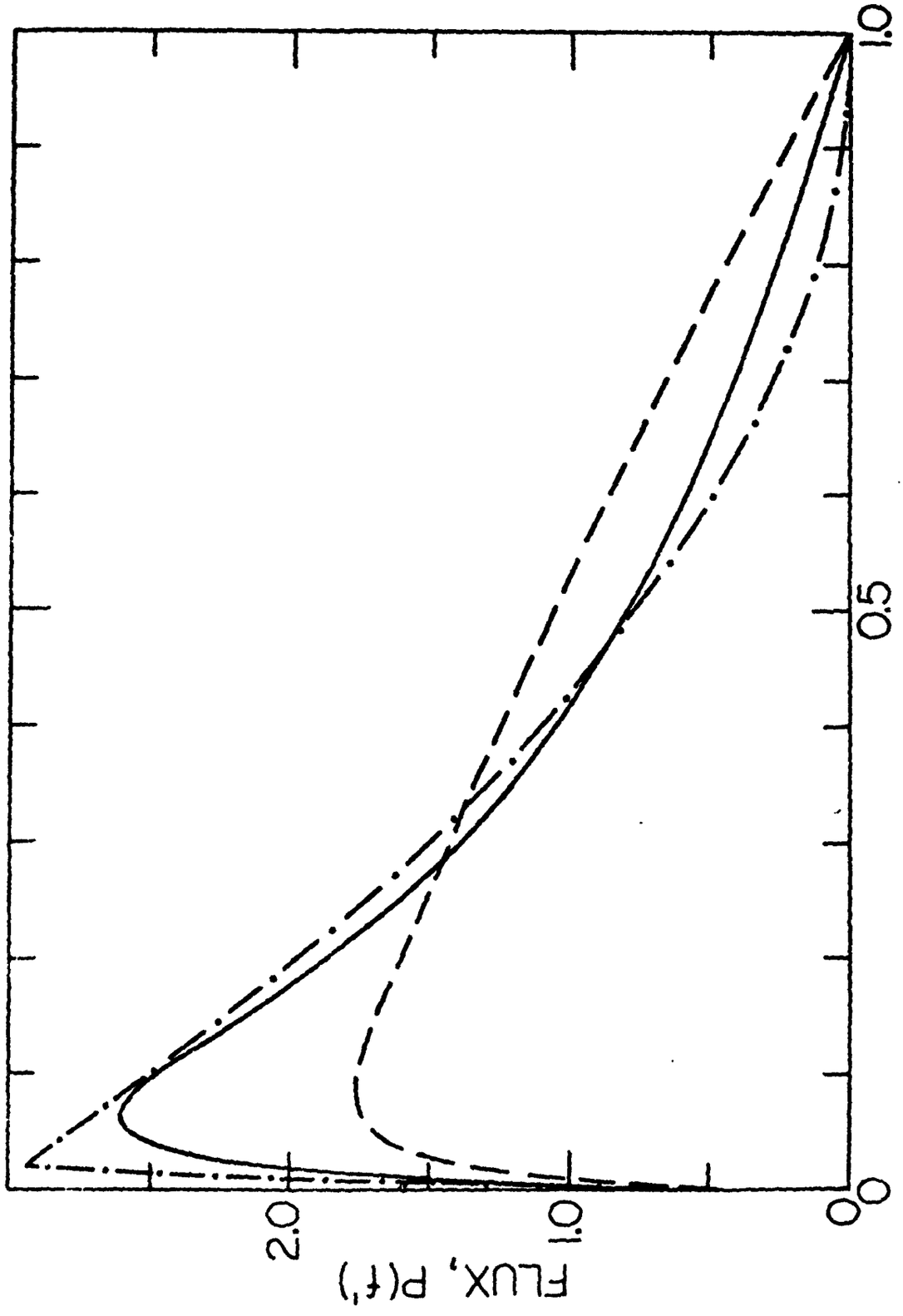

FIGURE 10(c)

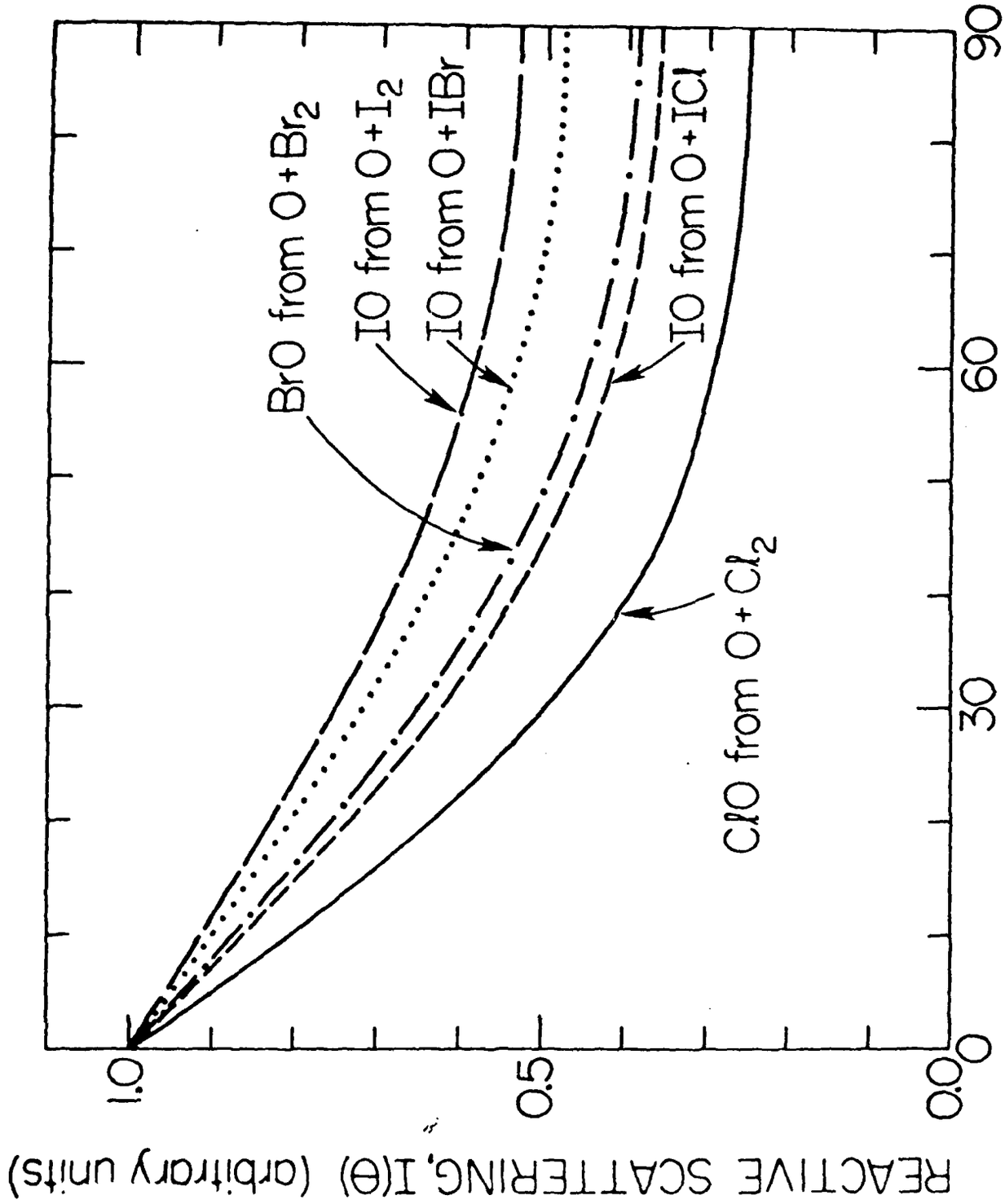
BrO from O+Br2
IO from O+I2
IO from O+IBr
IO from O+ICl
ClO from O+Cl2
1.0
0.5
0.0
0
30
60
90
CM SCATTERING ANGLE, Θ
REACTIVE SCATTERING, I(Θ) (arbitrary units)

FIGURE 11(A)

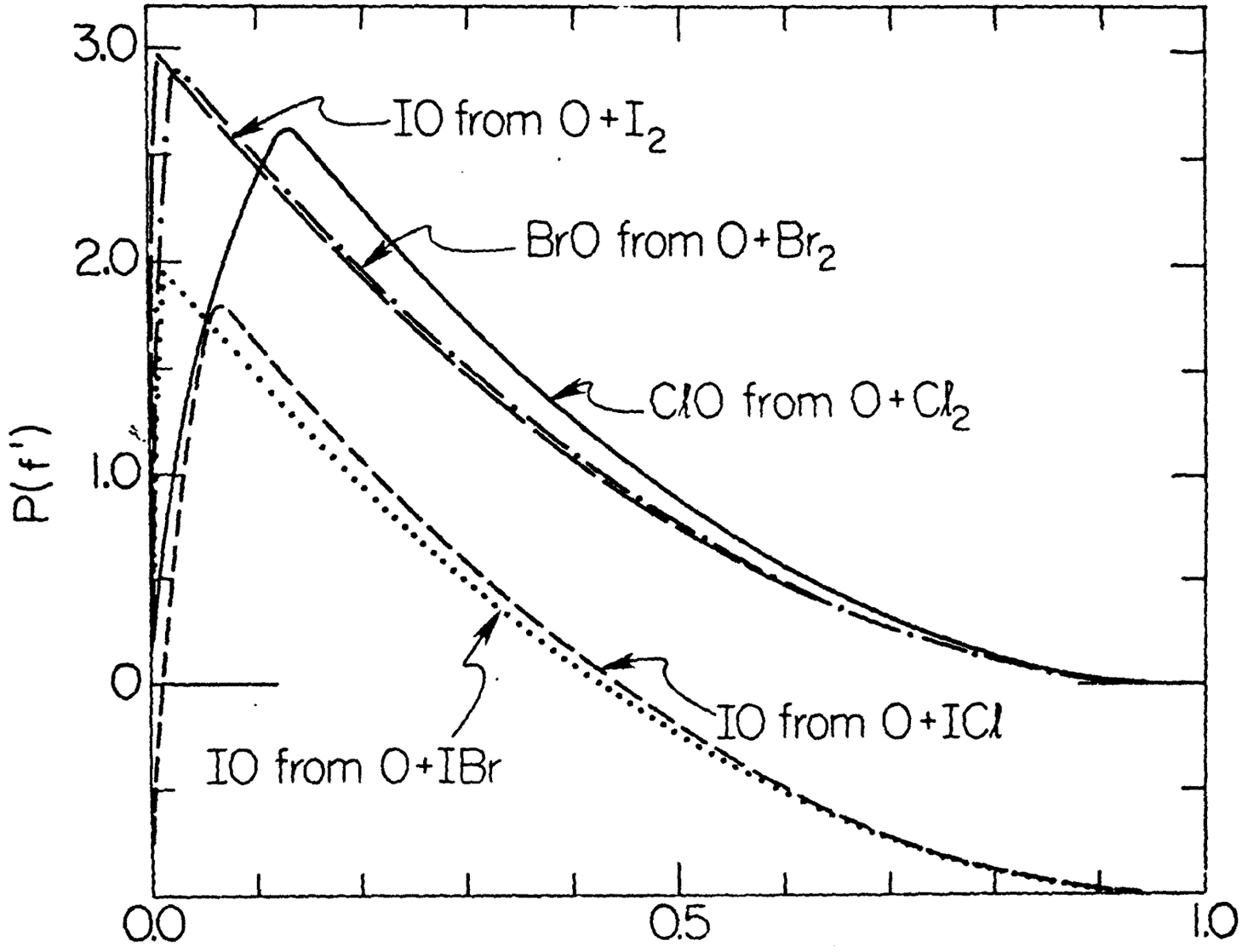
3.0
2.0
1.0
0
P(f')
IO from O+I2
BrO from O+Br2
ClO from O+Cl2
IO from O+ICl
IO from O+IBr
0.0
0.5
1.0
f'=ET'/ETOT, PRODUCT TRANSLATIONAL ENERGY

FIGURE 11(a)

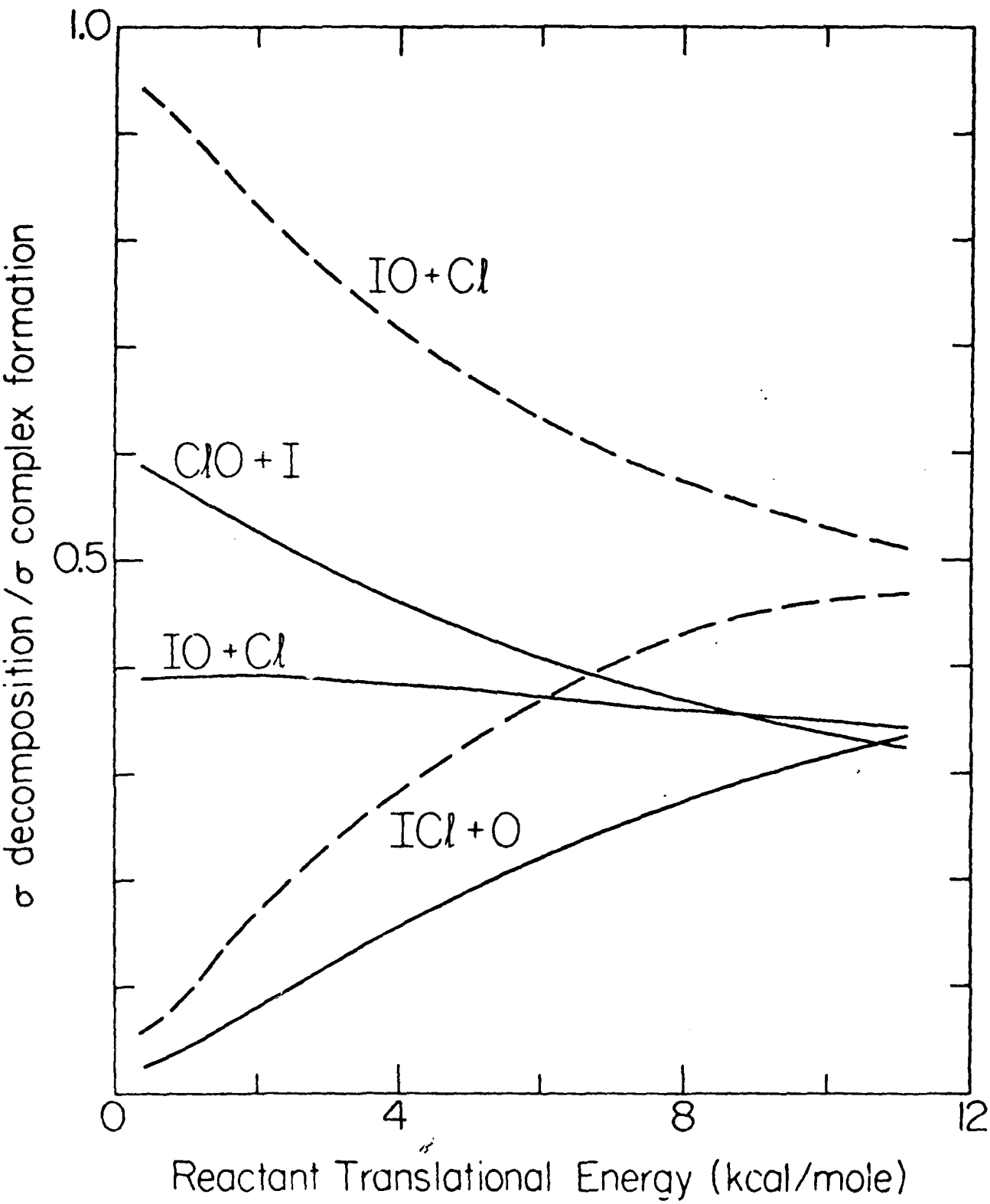
1.0
0.5
0
4
8
12
σ decomposition / σ complex formation
Reactant Translational Energy (kcal/mole)
IO + Cl
ClO + I
IO + Cl
ICl + O

FIGURE 12

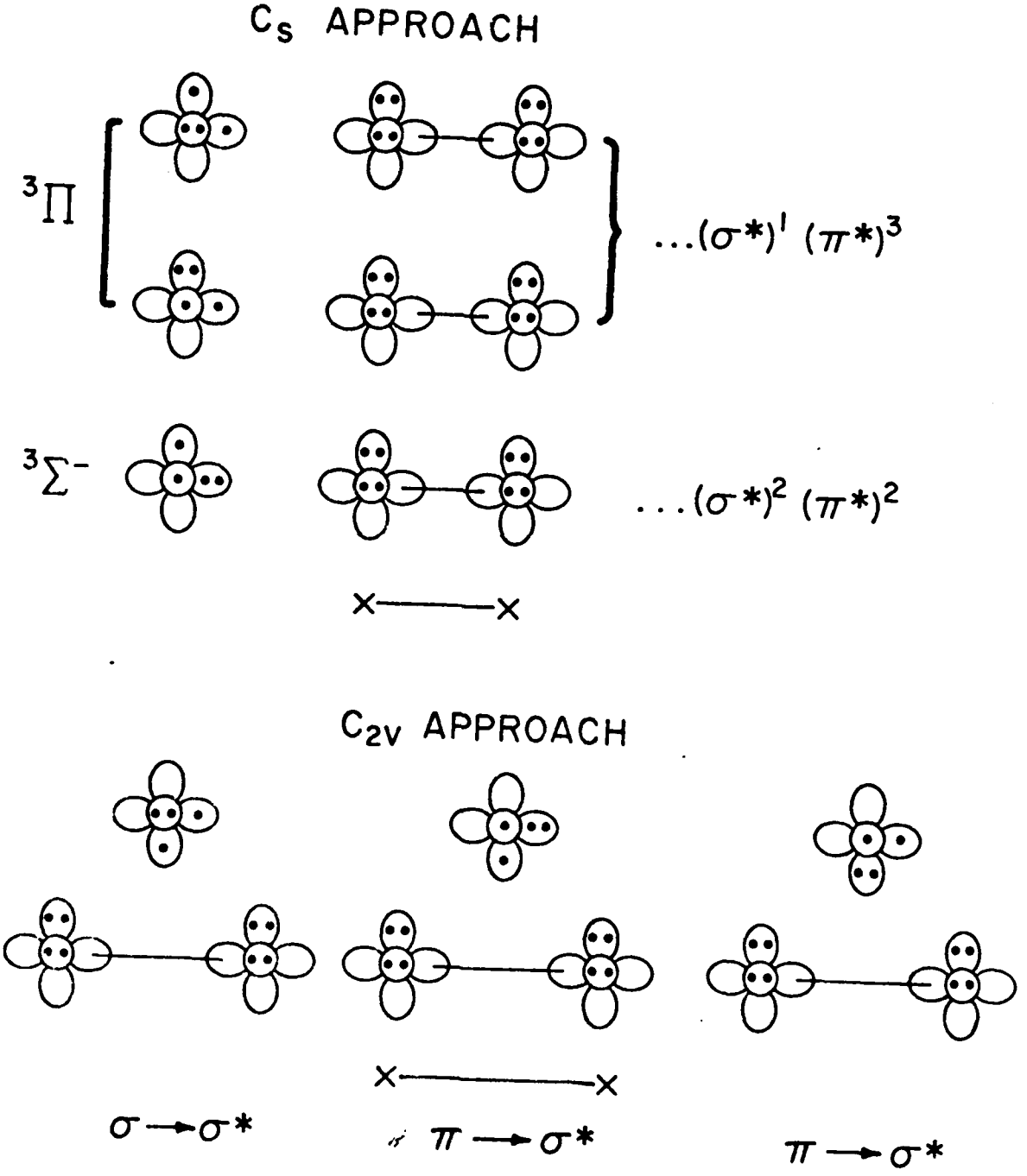
C_s APPROACH
$^3\Pi$
$\ldots(\sigma^*)^1\,(\pi^*)^3$
$^3\Sigma^-$
$\ldots(\sigma^*)^2\,(\pi^*)^2$
X——X
C_{2v} APPROACH
X——X
$\sigma \rightarrow \sigma^*$
$\pi \rightarrow \sigma^*$
$\pi \rightarrow \sigma^*$

FIGURE 13

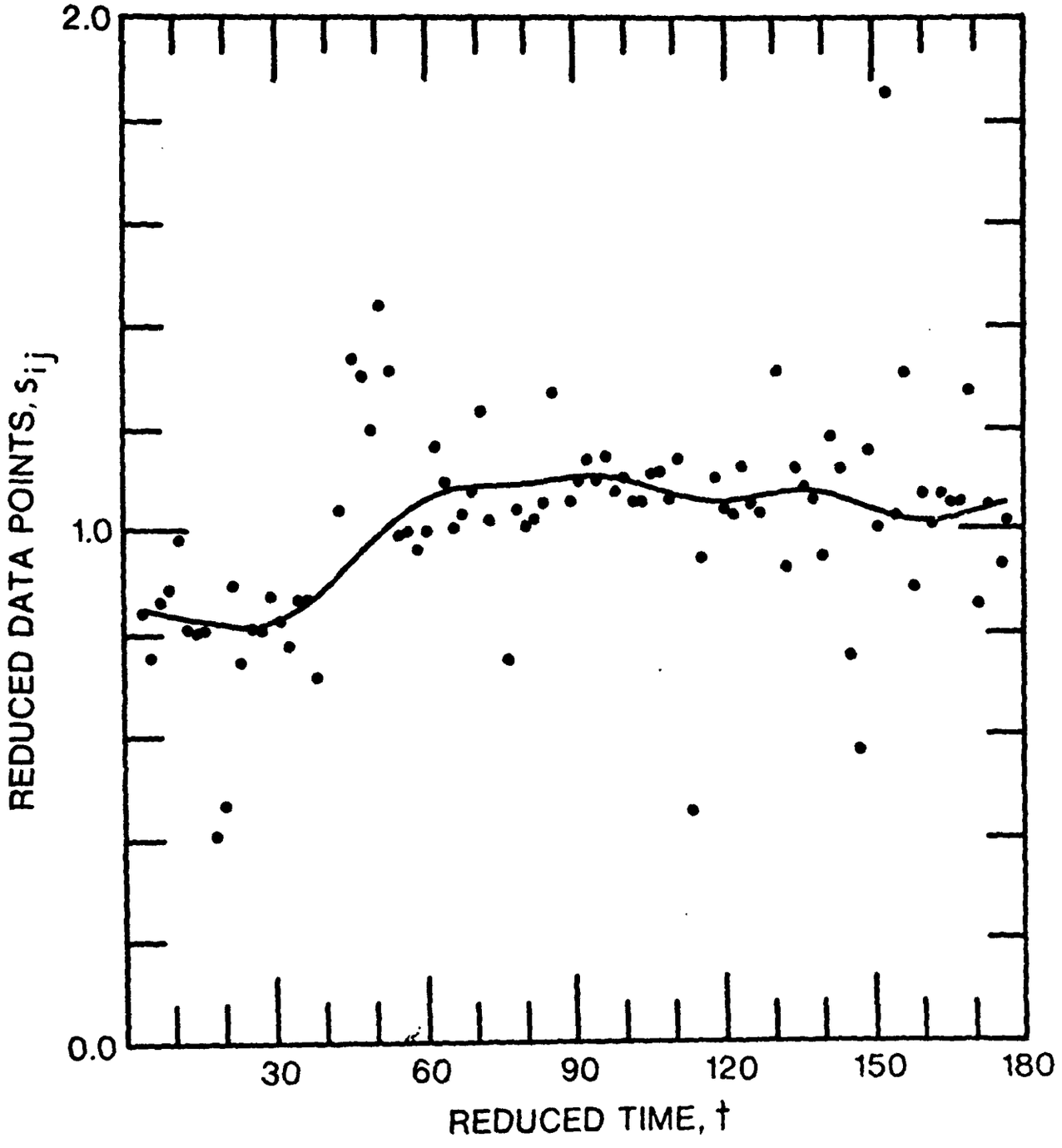
2.0
1.0
0.0
REDUCED DATA POINTS, s_{ij}
30
60
90
120
150
180
REDUCED TIME, $\dagger$

FIGURE 14

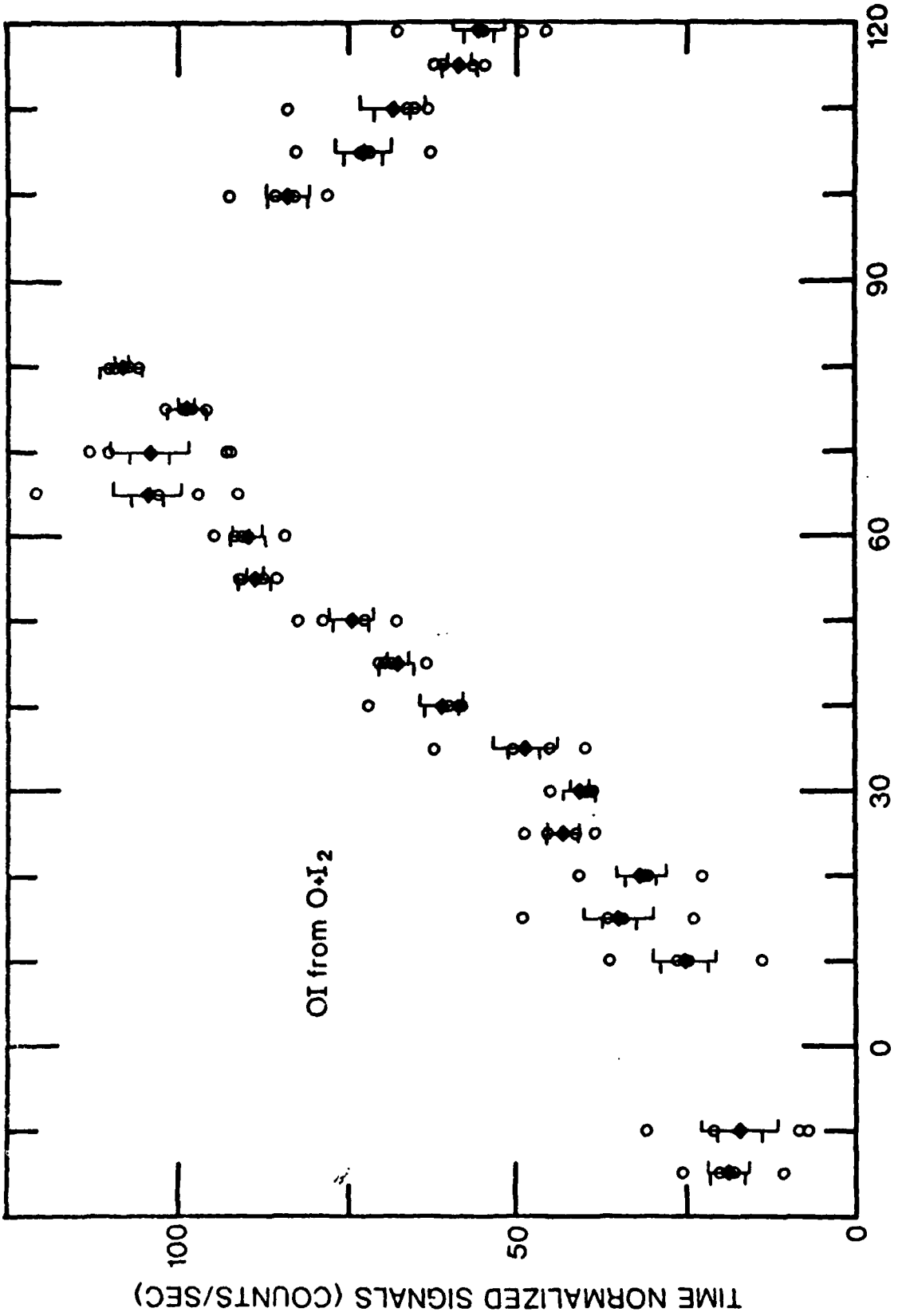
TIME NORMALIZED SIGNALS (COUNTS/SEC)
100
50
0
OI from O+I2
0
30
60
90
120
LABORATORY SCATTERING ANGLE, Θ

FIGURE 15

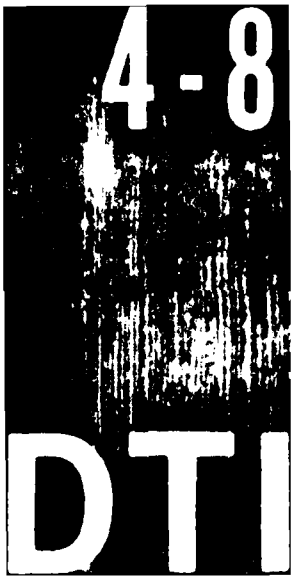
4-8
DTI